4D Printing of Liquid Crystals: What's Right for Me?

ADVANCED MATERIALS
www.advmat.de

4D Printing of Liquid Crystals: What's Right for Me?

*Marc del Pozo, Jeroen A. H. P. Sol, Albert P. H. J. Schenning, and Michael G. Debije**

Recent years have seen major advances in the developments of both additive manufacturing concepts and responsive materials. When combined as 4D printing, the process can lead to functional materials and devices for use in health, energy generation, sensing, and soft robots. Among responsive materials, liquid crystals, which can deliver programmed, reversible, rapid responses in both air and underwater, are a prime contender for additive manufacturing, given their ease of use and adaptability to many different applications. In this paper, selected works are compared and analyzed to come to a didactical overview of the liquid crystal-additive manufacturing junction. Reading from front to back gives the reader a comprehensive understanding of the options and challenges in the field, while researchers already experienced in either liquid crystals or additive manufacturing are encouraged to scan through the text to see how they can incorporate additive manufacturing or liquid crystals into their own work. The educational text is closed with proposals for future research in this crossover field.

1. Introduction

Materials science often looks for inspiration to the natural world for new materials or device design concepts. It can be argued that this also holds for fabrication procedures. One of the newest additions, additive manufacturing (AM), which builds larger objects from smaller elements, might well be interpreted as a throwback to our natural origins. This bottom-up approach is used by birds and termites, for example, to build their homes and nests from branches or dirt and saliva by adding elements one by one with specified arrangements, while spiders extract a processed polymer for building finely detailed webs. Humans build homes in a superficially similar fashion, orienting materials and depositing them piecewise into a larger, premeditated design; additively fabricating a house from mud, lumber, or brick.

The initial use of AM was for rapid prototyping of device designs, usually with inferior materials optimized for production speed at the expense of final material or device properties.[1] In development for about four decades, AM has now achieved greater public recognition, and is being applied in a growing variety of academic and industrial fields to produce performance materials and devices. More attention has been focused on the materials, as AM is beginning to be considered a manufacturing technique in its own right, its forte being ease of use (no large industrial machines are required), ease of model design (any personal computer can be used to generate designs) and a growing library of materials available for printing ranging from thermoplastics to cement.[2] Control of AM techniques is such that objects can be manufactured spanning from micrometers[3] to tens of meters:[2] consider the wide variety of current uses of AM, including in aviation,[4,5] biomedical and tissue engineering,[6–8] dietary,[9,10] construction,[2,11,12] garment design,[13] laboratory wares,[14,15] water purification,[16] and sensing applications.[17–19]

Most of the materials used in AM have essentially been static. What is needed are materials that can react to changes in their environment, autonomously altering their properties to perform untethered tasks, which are most desired for compliant soft robotics for healthcare,[20] or devices that work at the human–machine interface or for handling fragile objects.[21] This is where the term "4D printing" originates: a printed object generated using AM with stimulus-responsive materials (also called "smart materials"). Since both the geometry and responsivity of the materials can be tuned, impactful applications are envisioned for 4D printed devices.[22,23]

Many materials classes have been used for 4D printing, including (anisotropic) hydrogels,[24–27] shape memory polymers,[28] polysiloxane thermosets,[29] and liquid crystalline (LC) materials.[30–37] Hydrogels are a prime example, as they show large, reversible deformations based on swelling and deswelling cycles which can be programmed to respond to a number of potential triggers.[38–40] Hydrogel-based objects can be processed using a variety of AM techniques,[41] and when embedded with high aspect ratio dopants (cellulose fibrils, glass fibers), the devices can be made to actuate anisotropically.[24] However, hydrogels must be hydrated in order to function, which can pose an issue in dry or warm environments.

M. del Pozo, J. A. H. P. Sol, A. P. H. J. Schenning, M. G. Debije
Laboratory for Stimuli-Responsive Functional Materials & Devices (SFD)
Department of Chemical Engineering and Chemistry
Eindhoven University of Technology (TU/e)
Groene Loper 3, Eindhoven 5612 AE, The Netherlands
E-mail: m.g.debije@tue.nl
A. P. H. J. Schenning
Institute for Complex Molecular Systems (ICMS)
Eindhoven University of Technology
Groene Loper 3, Eindhoven 5612 AE, The Netherlands
The ORCID identification number(s) for the author(s) of this article can be found under https://doi.org/10.1002/adma.202104390.

DOI: 10.1002/adma.202104390

Polysiloxane thermosets, when doped with high aspect ratio glass fiber fillers, have been shown to yield objects with preprogrammed deformation in dry environments.[29] Similar to the hydrogels, these composites can be engineered so that preprogrammed bending occurs. Despite these polysiloxane thermosets showing reversible preprogrammed actuation in dry environments, they lack versatility in terms of material properties.

Shape memory polymers (SMPs) are a popular material class, already having been widely demonstrated as 4D printing materials.[42–46] SMPs are mechanically programmed during a temperature cycle; a subsequent temperature cycle releases the built-up strain, resulting in actuation. Compared to hydrogels, higher moduli actuators capable of performing greater specific work can be achieved, and actuation in dry environments is possible. Similar to hydrogels, a variety of AM techniques have been used to deposit the material, including drop-on-demand inkjet printing methods.[45–47] Unfortunately, however, in most cases shape memory polymers cannot cycle between actuated and unactuated states autonomously and need to be reprogrammed after each actuation stroke, known as "one-way" shape memory. There is only a select group of SMPs that undergo "two-way" actuation.[48,49]

LC-based materials combine the characteristics of all these materials, allowing preprogrammable, reversible, anisotropic actuation in both dry and wet environments while having tunability in terms of material properties. LCs have a proven track record as "smart" materials in a wide variety of application fields, including water purification, optical sensing, display technology, energy management, and as artificial muscles.[48,50–57] Despite LCs being a recent addition to the materials library used in 4D AM, they are already proving to be an appealing alternative to the conventional stimuli-responsive materials employed.[31–33,35,36,58–63]

This work fills a gap, serving both as literature review and a tutorial for people looking to enter 4D printing of LC-based materials from either field. We critically select research reports in a didactic format, so novices from either the fields of responsive LCs or AM (or both) may select specific sections to learn how to make informed choices of AM technique and design a corresponding functional LC mix to allow for exploration of novel 4D printed LC-based devices on the micrometer to centimeter scales. The structure of this work may be seen in **Figure 1**. By introducing the entirety of the field in an easily-digestible manner, we hope to give appreciation for the scope of the field and provide a "cookbook" in terms of fundamentals in both materials choice and printing techniques, as well as inspire new parties to join in this exciting research area. We also present the boundaries of existing experience and offer possible roadmaps toward future developments.

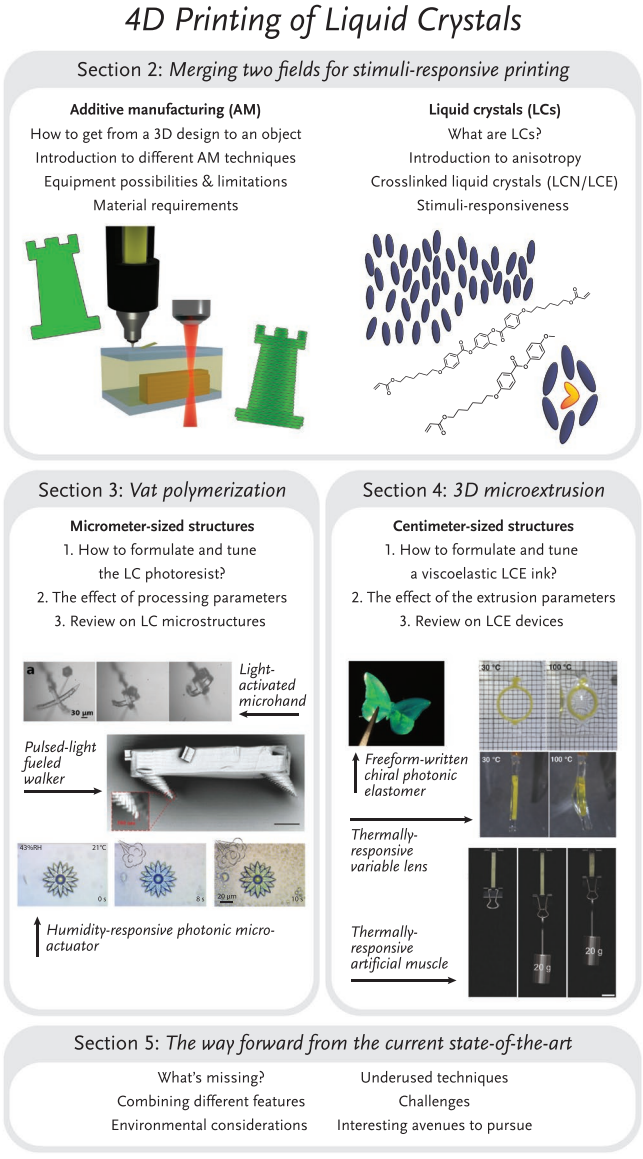

Figure 1. Visual table-of-contents. First, we present the basic theory for additive manufacturing techniques and LCs (Section 2). Then we discuss how to process, formulate, and tune LCs for their use in two different AM techniques: vat polymerization (Section 3) and 3D microextrusion (Section 4). Different examples that embody the achievable stimuli-responsive devices possibilities via AM of LCs are shown. At the end (Section 5), we offer a reflection of what direction research could take from here. The light activated "microhand" micrographs: Adapted with permission.[30] Copyright 2017, Wiley-VCH. The pulsed-light fueled walkers electron micrographs: Reproduced with permission.[31] Copyright 2015, Wiley-VCH. The humidity-responsive photonic micro-actuator micrographs: Adapted under the terms of the CC-BY Creative Commons Attribution 4.0 International license.[59] Copyright 2020, American Chemical Society. The freeform-written chiral photonic elastomer image: Reproduced under the terms of the Creative Commons CC BY license.[64] Copyright 2021, Wiley-VCH. The thermally responsive variable lens images: Adapted with permission.[36] Copyright 2017, Wiley-VCH. The thermally responsive artificial muscle images: Adapted with permission.[34] Copyright 2018, Wiley-VCH.

2. Merging Two Fields: Toward 4D Printing of Liquid Crystals

This section has two goals. First, illustrating the available 3D printing techniques, with emphasis on those that have already been used in combination with LCs, but also discussing procedures we feel hold promise for future materials research but which have not yet been tested with LC materials. Second, because LCs are a class of stimuli-responsive materials that have many adjustable properties (mechanical, e.g., glassy or rubbery network at room temperature (RT), anisotropic contraction/expansion; optical, e.g., birefringence; and in stimulus response, e.g., response to light, temperature or humidity) we will

offer a concise description of LCs together with information on how to use them and how to adapt their properties to the requirements of one's intended application and AM technique. After completing this section, we believe the reader will be equipped with the tools necessary to make appropriate choices of LC material and AM equipment for their intended application.

2.1. Additive Manufacturing Techniques

Over the past four decades, since the introduction of stereolithography (SLA)[65] and fused filament fabrication (FFF, also commercially known as "fused deposition modeling," FDM),[66] additive manufacturing has been the umbrella term encompassing 3D printing techniques. These techniques can be classified in different branches, but all have one thing in common: fabrication of 3D objects by depositing and/or solidifying material in place, rather than sculpting an object out of a larger material block. The process always starts with a computer-assisted design (CAD) which is "sliced" into layers using software that generates a fabrication instruction file for the printing equipment (**Figure 2**) written in "G-code." When creating this instruction file, decisions are made affecting the structure's fidelity to the CAD design (degree of correspondence of the final print to the intended structure in the CAD model) and its physical integrity (the physical "stability" of the print resulting from proper adhesion between layers). Depending on the layer thickness chosen, less or more layers are used in fabrication: the more layers, the more faithful the final object to the original design. In some techniques, the layer "infill" also needs to be defined, the infill being the track pattern which the individual physical print lines follow in building the layers. There are several options for infill: rectilinear, concentric, or triangular, among others (Figure 2). For anisotropic materials aligned by the print path direction, such as liquid crystal elastomers (LCE),[34,36,67] the type and density of infill can strongly affect the final mechanical properties in all three spatial dimensions (Section 4). What determines the technique best used for the print is dictated by the structure's dimensions and the properties of the materials chosen to create it. As shown in the drawing, in each step of the process different decisions are made which affect the final structure.

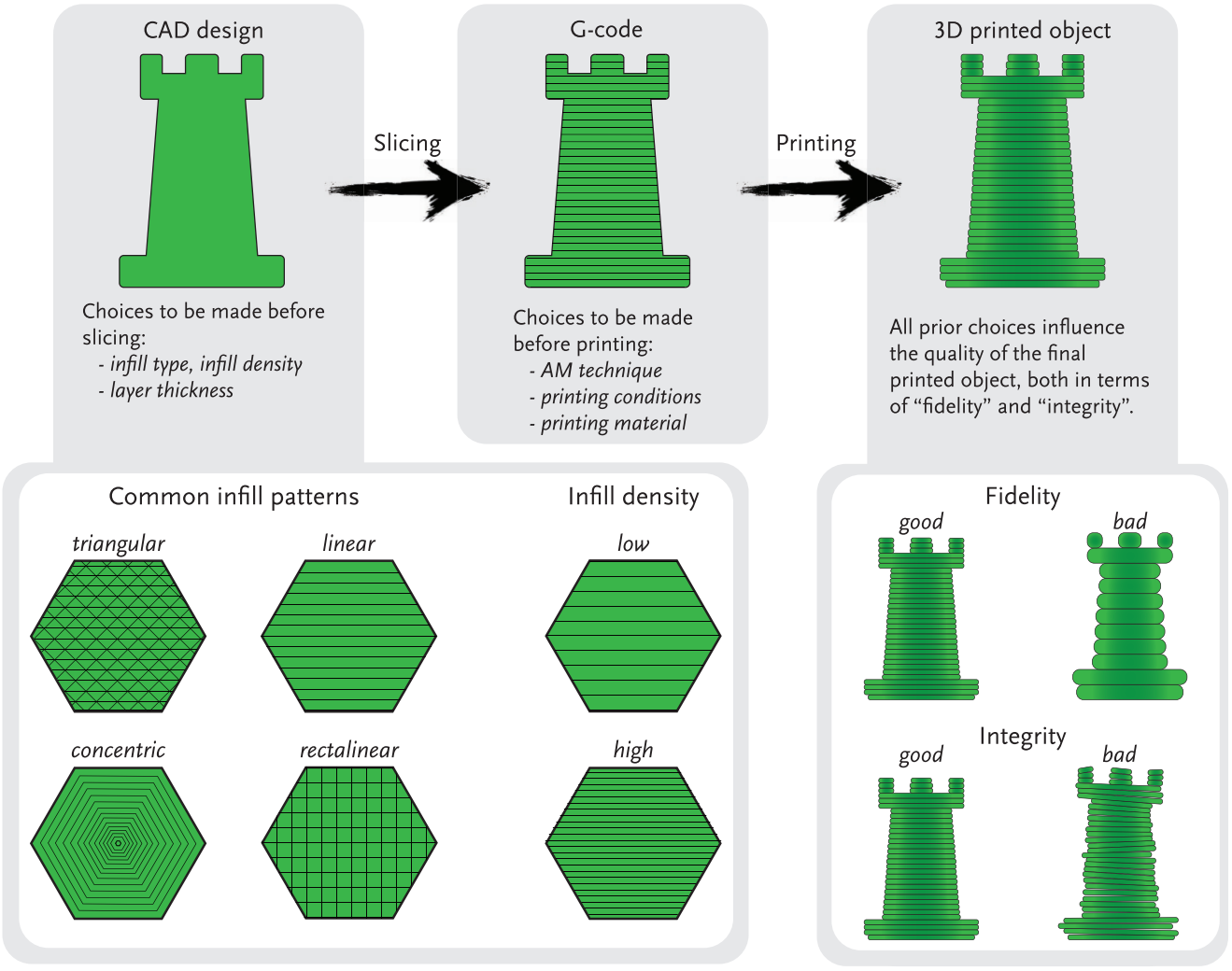

Figure 2. Schematic describing the process from a CAD design to a 3D printed object.

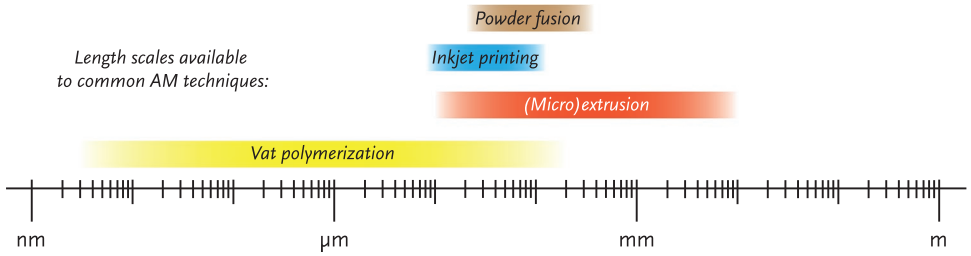

Figure 3. Overview of the most common additive manufacturing type classified by the resolution typically achieved.

For fabrication of LC-based 3D objects, two categories of AM techniques have been primarily used: vat polymerization and 3D microextrusion.[30–32,34–37,58,59,63,68,69] Each branch is suitable for specific classes of LC monomers. Vat polymerization is appropriate for low molecular weight mesogens, and 3D microextrusion for mesogenic oligomers (Section 2.2.2 for different types of LCs used in AM). For each technique there are equipment options, each with different resolution as shown in **Figure 3**. Vat polymerization tends to have a higher resolution than microextrusion, and so it is often used for fabrication of microstructures, while 3D microextrusion is typically employed for millimeter to centimeter scale objects. These two branches will be discussed in Sections 2.1.1 and 2.1.2: for further reading on alternative printing techniques, the reader is directed to the reference literature.[1]

2.1.1. Vat Polymerization

In vat polymerization, localized crosslinking is induced in a bulk of a light-sensitive material, typically known as the "photoresist," using light of specific wavelengths, with a resolution generally between 0.1–100 μm.[1] The achievable resolution is influenced by both the material polymerization speed and diffusion rate. A fast polymerization increases accessible fabrication speed and reduces the polymerization voxel size, this being the volume unit in which the polymerization occurs, which in turn increases the resolution. To achieve rapid polymerization, low molecular weight reactive mesogens (RMs) with acrylate and epoxide groups are typically used since they have a lower viscosity than mesogenic oligomers (see Section 2.2.2) and can be aligned in the vat using different techniques. A low diffusion rate of the activated reactive groups is often accomplished by either an increase in photoresist viscosity or by adding polymerization inhibitors, reduces the polymerization voxel size. Furthermore, the low viscosity allows easier removal of the unreacted monomer and/or extraction of the final object from the vat.

SLA is the progenitor of light-based layer building techniques.[65] In SLA, a focused laser, typically ultraviolet (UV), scans through a vat of photopolymerizable resin. The laser follows a predefined path per object layer, locally initiating the crosslinking of the resin. Since the laser initiates polymerization only a few micrometers into the resin vat, lifting the object away from the plane of polymerization after a layer hardens is required. This allows unreacted resin to fill the gap vacated by the newly polymerized region of the object, allowing formation of the subsequent layer. Following this process, a layer-based 3D object is fabricated. Owing to the small spot size of laser beam, the resolution of SLA is between 25–100 μm.[1] However, this resolution comes at the expense of longer printing times, especially when fabricating centimeter scale objects. More recently, digital light processing (DLP) equipment has reduced the printing time by changing the way the layers are polymerized. Rather than scanning the laser through the photoresist to form a layer, the light source illuminates the resist with the geometry of the entire layer at once, similar to photolithography, but using a digitally programmable mask. The mask may be changed repeatedly to project the shape of the layer, reducing the printing time. However, since DLP uses physical pixels to form this digital mask, typically a liquid crystal display (LCD) screen, the achievable resolution is limited to ≈100 μm.[70]

Two-photon polymerization direct laser writing (TPP-DLW), also known as "multiphoton lithography," is similar to SLA, but rather than single-photon initiation of the crosslinking reaction, it relies on the nonlinear optical process of "two-photon absorption" (TPA). TPA requires an extremely high photon density, as two photons need to be simultaneously absorbed. This high photon density can be achieved by focusing a femtosecond laser, typically a ≈780 nm fs-pulsed Ti:sapphire, which concentrates the photons temporally; by using a microscope objective to focus the light, the photons are also concentrated spatially. The photon flux is the greatest at the focal point and exponentially decreases from there. Only at the focal point is the density of photons high enough for TPA to occur, implying polymerization only occurs at the focus. By scanning the focal point through the bath of material, polymerization can be induced anywhere in the resist bath, a feature not possible with SLA or DLP in which polymerization can only occur at the surface of the vat. The 3D focal point has an ellipsoidal shape, with an equal length in the x- and y-axes, typically around 60 nm, and slightly elongated in the z-axis, this being ≈180 nm;[71] both the shape and dimensions are influenced by the laser intensity and the numerical aperture (NA) used.[72,73] Because of the small dimension of the focal point, the resolution of this technique is ≈20 nm to 5 μm:[1,74,75] final resolution is critically dependent on both the material and the printing parameters (Section 3.1). After the fabrication exposure steps, any unreacted monomer is typically removed during a "developing" step to obtain the final object.

2.1.2. 3D Microextrusion

In extrusion-based equipment, a thread of material known as a "filament" is forced through a nozzle and deposited on a substrate or previously printed layer in a predetermined

fashion. Layers are formed line-by-line, and objects layer-by-layer. The resolution, from 100 µm to 1 cm,[1] is primarily determined by the nozzle diameter and printing speed. Smaller nozzle diameters reduce the diameter of the deposited fiber and so increase the resolution. However, when reducing the nozzle's diameter, the pressure required to extrude the materials increases, so the viscoelastic properties of the material naturally limit the practical resolution that can be achieved. Apart from the nozzle diameter, the minimum step that the print nozzle can move in *x*, *y*, and *z* also limits the achievable resolution of the structures. Moreover, in some cases, the printing speed can influence the amount of material deposited in one location. If fast printing speeds are used, the diameter of the fiber is reduced; but some printers can correct for this to deliver the same volume of extruded material at faster speeds.

Once extruded, the material must be able to maintain its shape. This excludes low viscosity materials and makes thermoplastics and viscoelastic thermosetting resists more appropriate for 3D microextrusion equipment. Since common reactive LC oligomers are viscoelastic thermosets, they are a better option to use as inks in extrusion-based techniques than lower molecular weight, runny LC monomers (Section 2.2.2). For these more viscous LC inks, directional orientation of the molecules in a premeditated manner has been shown through programming the infill (Section 4).[34,36,76] The alignment under the influence of the flow conditions during extrusion eliminates the need for doping with anisotropic fillers such as the glass fibers or cellulose nanocrystals required to orchestrate differential swelling in hydrogels.

FFF and direct ink writing (DIW) are the two main techniques for 3D microextrusion. Of these, FFF is probably the most widely recognized, owing to its commercial status and ease-of-use. FFF works with thermoplastics which are stored as spools of solid polymer. During printing, this spool is fed through a feeder which drives it into the printing nozzle where the polymer is heated to above its melting point (T_m). The molten material is pushed through the nozzle, which typically has a diameter of 400 µm, by the incoming solid filament. Through *x*, *y*, and *z* movement of the nozzle, the printing bed, or both, material is deposited as dictated by the computer-generated G-code. On the bed, the material solidifies into the final, hard polymer object. The shear and elongational flows present during extrusion can help align the polymer chains in suitable feed materials,[69] leading to highly anisotropic material properties, including tensile modulus and strain-at-break which are often considerably greater when gauged in the printing direction.

DIW, first mentioned as a technique to fabricate ceramic objects in complex, 3D shapes,[77] is suitable for materials that cannot be stored as a solid filament. The syringe is loaded with a viscoelastic ink: a thermoplastic polymer melt, a resist, or materials such as polyelectrolyte complexes or ceramic suspensions.[78] The syringe is pressurized mechanically or pneumatically and, like FFF, a predefined print path is followed by the printer to write the material in place. Drying or curing of the material can be performed during the print process after each layer is deposited, or after the entire print is completed, depending on the material requirements.

2.2. Liquid Crystals

Over the past 50 years, advances in the LC field have expanded them out of LCDs and into functional devices of all kinds, and now into the AM world as mentioned in Section 1. As materials that can be molecularly aligned, they are the ideal constituents for bottom-up construction of responsive objects. Situated between ordered solid and isotropic liquid phases (abbreviated as "I" or "Iso" in the LC literature) the LC phases combine molecular orientational order with the ability to flow and reorient when an appropriate trigger is imposed, first seen over 150 years ago.[79–81] This stimuli-responsive molecular reorientation is the basis of their wide applicability in stimuli-responsive, "smart" materials.[50] In the 1970s, the first compounds with liquid crystalline properties at RT were developed for LCDs,[82] which also ushered in a time of wider applicability of this class of matter. Since then, many different LCs have been developed for a variety of applications, as well as LC mixes aimed specifically for AM techniques.

LC phases are also called "mesophases" (after ancient Greek μέσος, mésos, "middle, between"), and the molecules "mesogens." LC phase behavior can be a function of temperature ("thermotropic"), or for those that occur in solution, dependent on both temperature and concentration of LC in the host medium ("lyotropic").[83] Thermotropic mesogens have strongly anisotropic geometries, whether disc-shaped ("discotic") or rod-like ("calamitic") (**Figure 4**a), although there are even more possibilities, such as bent-core.[84]

In this work, we consider only thermotropic, calamitic LCs, and their uses, given their leading position in stimuli-responsive materials for 4D printing.[50,54,85,86] Additionally, there are liquid crystal polymers (LCPs) that are not liquid crystalline in bulk at room temperature like the low-molecular weight molecules discussed here, but show LC phases during processing. The initial molecular alignment is retained which gives these materials, such as polyaramids, their exceptional anisotropic mechanical properties.

Low molecular weight calamitic mesogens are conventionally constructed from a stiff core built using a (series of) ringed structures (phenyl, pyridyl, cyclohexyl) substituted with flexible alkyl chains of variable lengths, typically C_3 up to C_{12} (**Figure 5** for examples). Given a suitable environmental temperature, these mesogens self-organize into a nematic phase (N) wherein the molecules display orientational order; some mesogens can form one of many smectic phases (Sm), which combine orientational with spatial ordering (Figure 4b). The averaged direction of the molecular long axes of the mesogens is described as the molecular director (**n**) (Figure 4c). Numerically, the degree of alignment order can be described with the order parameter (*S*), defined as

$$S = \left\langle \frac{3\cos^2(\theta) - 1}{2} \right\rangle \tag{1}$$

with θ being the tilt of a mesogen relative to **n**. Typical nematic mesophase *S*-values are 0.5 to 0.6,[56] with smectics having slightly higher order (0.7–0.8).[87] *S* can be determined using optical[88] or X-ray scattering[89] methods.

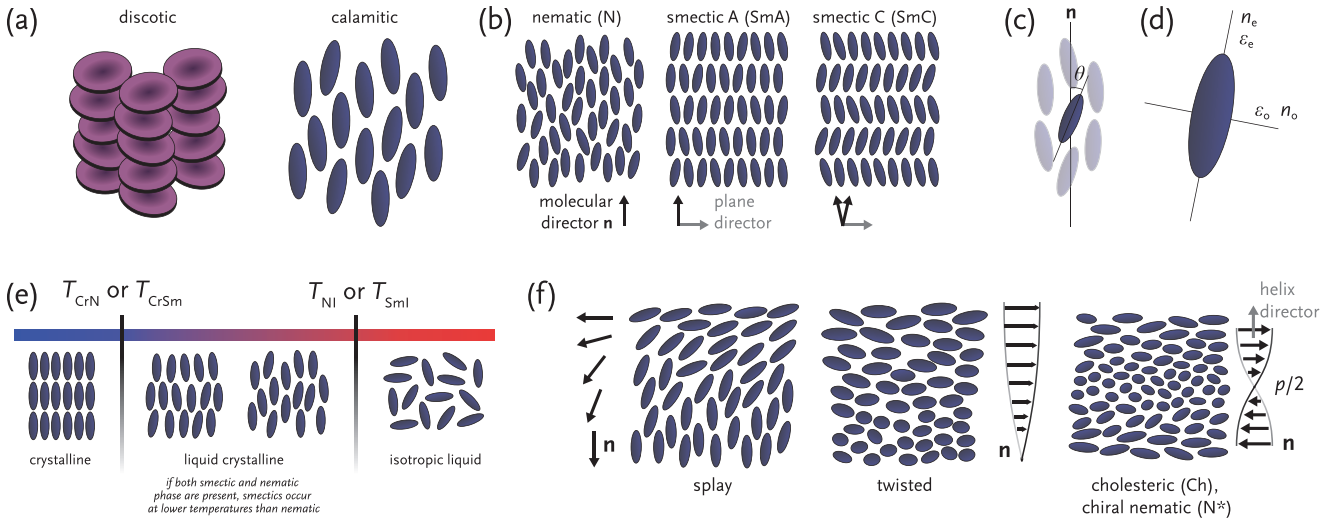

Figure 4. Schematic drawings of a) discotic and calamitic mesogens in an unspecified mesophase. b) Typical calamitic mesogen alignments in the nematic (N), smectic A (SmA), and smectic C (SmC) mesophases. Visualized underneath are the molecular directors **n**. c) Molecular orientation and angle θ with respect to the molecular director **n**. d) Orientation of ordinary (n_o) and extraordinary (n_e) refractive indices and relative permittivities (ε_e, ε_o). e) Generalized temperature-dependence of calamitic mesophases between crystalline solid and isotropic liquid. f) Splay, twisted, and chiral nematic/cholesteric (N*/Ch) director configurations and the associated local molecular directors **n**. Also shown for cholesteric is $p/2$, half the length of a full 360° rotation (the "pitch") of **n**.

As a result of the anisotropic shape of calamitic molecules, the dielectric properties are also anisotropic, a trait at the root of the "smartness" of many LCN-based devices. This is expressed as two orthogonal relative permittivity values, extraordinary (ε_e) and ordinary (ε_o). Depending on the difference, $\Delta\varepsilon = \varepsilon_e - \varepsilon_o$, the mesogens will reorient along ($\Delta\varepsilon > 0$, positive dielectric) or against ($\Delta\varepsilon < 0$, negative dielectric) imposed electric fields. The inherent link between ε and index of refraction (n) means that LCs also have two refractive indices, extraordinary (n_e) and ordinary (n_o), which when the mesogens are aligned over large length scales, expresses itself as birefringence ($\Delta n = n_e - n_o$) (Figure 4d). This birefringence allows users to swiftly recognize alignment patterns and mesophases by observing samples held between crossed polarization filters. As an example, a well-aligned planar nematic sample is recognized by observing a bright transmission when **n** is positioned at a 45° angle to the transmission axes of crossed polarizers, and a dark appearance when **n** is aligned parallel to one of the two filters. Since optical recognition of other mesophases can be quite challenging, we refer the reader to reference literature on this subject.[90]

2.2.1. Liquid Crystal Alignment

The molecular order is an important characteristic of LCs that has a direct effect on the quality of its anisotropic properties and how it responds to external stimuli. Thus, controlling the molecular alignment during the 3D printing process is imperative. Here we will describe common ways to align the mesogens since these set the basis on how the molecules are aligned in different AM techniques.

The mesogenic orientation can be homogenized at the macroscale by imposing boundary conditions. These boundary conditions can be obtained via treating the substrate surface(s) chemically, applying electric or magnetic fields, or using mechanical force fields such as shear or elongation. AM techniques where the LC is in a vat generally use treated surfaces in the vat or electric/magnetic fields across it. Extrusion-based AM, FFF and DIW, mostly depend on process-inherent elongation and shear of the ink for alignment.

Chemical surface treatments in the form of polymeric alignment layers grant considerable freedom. The classic method is to make a glass cell with alignment layers on the top and bottom surfaces.[85] After filling the cell at the isotropic temperature, it is cooled to the LC phase, and then slowly to RT (Figure 4e). Due to the boundary conditions imposed by the alignment layers, when the molecules undergo the phase transitions from isotropic to LC, they self-organize in the predetermined way. Depending on the alignment layer(s) used, mesogens can be aligned parallel ("planar")[31] or perpendicular ("homeotropic") to the substrate,[91] "splay" (with mesogens aligned parallel to the surface plane at one side and perpendicular to the surface plane at the other),[30] "twisted" (with the mesogens at different surfaces pointing in different directions),[92] or with a continuously twisting molecular director, known as "cholesteric" alignment which is induced chemically instead (Figure 4f).

When using electrically addressable LC mixtures, the alignment of the molecules can be controlled by an electric field. Typically, a cell with an alignment layer and transparent electrodes such as an indium tin oxide (ITO) is used.[32,93–95] Normally, the alignment layer induces a planar alignment in the LC. When a sufficient voltage is applied between the electrodes, the resulting electric field reorients the positive dielectric molecules from a planar toward a tilted alignment at intermediate potentials and near homeotropic (normal to the surface) alignment at high potentials. Using this approach, in situ control of the alignment of the LC is obtained.[32,94] The ITO electrode can also be of an interdigitated design, which may be used to create more complex alignments.[96]

Using the mechanical force fields (shear or elongation) can also align LCs. This method of aligning the mesogens has the

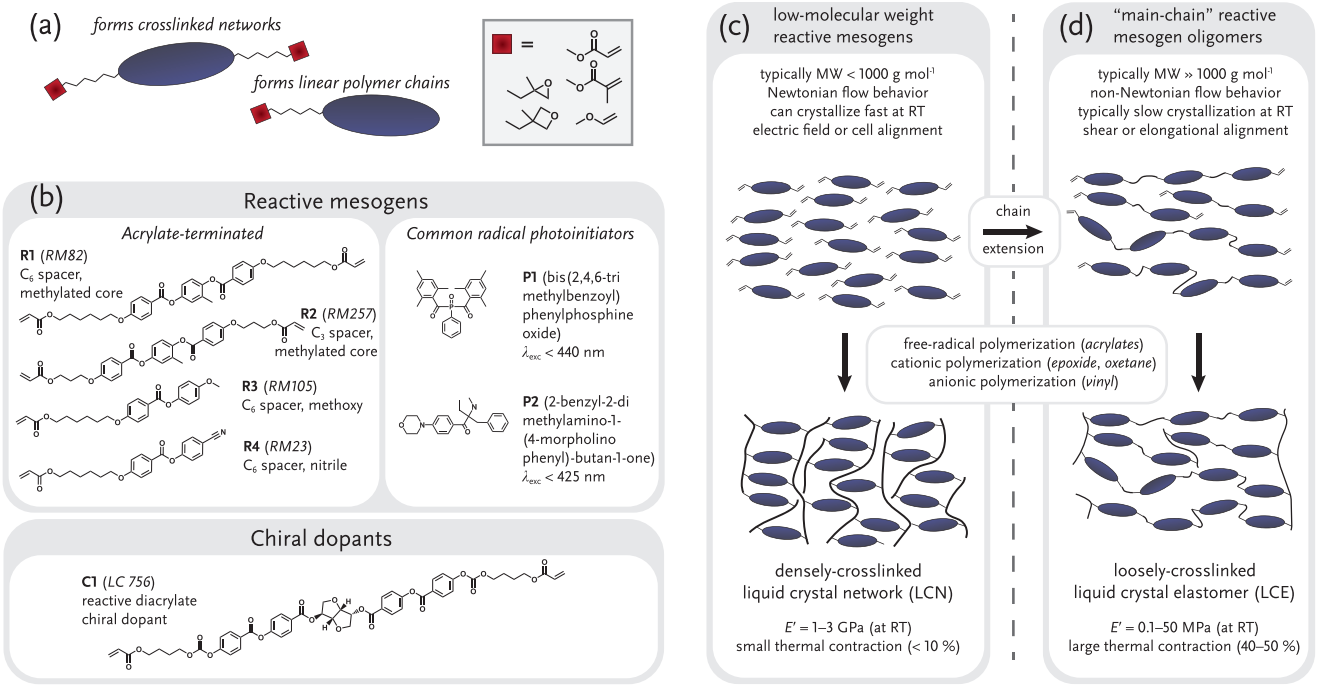

Figure 5. a) Visualization of reactive mesogens (di- and mono-substituted) and the reactive functional groups commonly encountered. b) Molecular structures and common names of some typical mesogens used in reactive LC research. Full names can be found in Tables S1–S4 in the Supporting Information. c,d) Schematic drawings of the monomers used to make LCNs and LCEs and characteristic figures defining each class. Idealized network structure for LCNs and LCEs after crosslinking, and common mechanical properties.[54]

disadvantage of only being capable of aligning the LCs parallel to the mechanical field, making splay or twisted nematic alignment unattainable. Given their increased viscosity, elongation and shear are the primary means of molecular alignment of LCEs and LCPs in extrusion-type AM (Section 4): the mesogenic cores orient along a single uniaxial direction through these force fields and are then fixed by polymerization.

A self-induced helicoidal alignment pattern in the bulk of the material can be attained by adding a chiral molecule to a nematic LC. This forms a chiral nematic (N*), or "cholesteric" (Ch), phase. Formation of this phase is complicated by shear forces imposed during deposition, but the proper alignment can be recovered by allowing the helices time to form before fixing by polymerization. When the periodicity of the mesogenic rotation is at the same scale as the wavelength of light, selective reflection of light can occur, similar to a 1D Bragg reflector,[53] but in this case the circular polarization of the reflected light matches the helical pitch of the cholesteric, either right- or left-handed. The birefringence of the host LC determines the width of the reflection band, while the concentration of chiral dopant dictates the central wavelength of reflection. The alignment periodicity is quantified with pitch length p, which is the distance taken for a 360° rotation of **n** along the helix director (Figure 4f). For reflection in the visible region of the electromagnetic spectrum, this means p is required to be in the hundreds of nanometers. Multiple factors influence the reflected wavelength (λ_{max}) and width of the reflection band ($\Delta\lambda$), these being the average refractive index of the LC ($\langle n \rangle$), "helical twisting power" (HTP) of the chiral dopant, and its weight fraction (x). These are connected through the following equations

$$\langle n \rangle = (n_e + 2n_o)/3 \tag{2}$$

$$p = (\mathrm{HTP} \cdot x)^{-1} \tag{3}$$

$$\lambda_{max} = p\langle n \rangle \cos(\theta) \tag{4}$$

$$\Delta\lambda = (n_e - n_o)\, p \tag{5}$$

The helical twisting power is perhaps the most abstract variable in this set. Briefly, it is a property deriving from the unique interactions between the chiral dopant species and the LC mixture, defined with units μm^{-1}. Larger HTP means a lower weight fraction is required to reflect a given wavelength, while the sign of HTP indicates whether the resulting helix is left-handed (–) or right-handed (+).

2.2.2. Liquid Crystal Networks (LCNs) and Elastomers (LCEs)

Macroscopic expression of liquid crystalline properties, such as birefringence and thermal contraction, requires the presence of molecular ordering. Normally, this only occurs in the LC mesophases, which are situated at defined temperature ranges. This temperature range can be extended by fixing the molecular alignment of the mesogens into a "permanent," chemically bound polymer network. Calamitic RMs, LC mesogens modified with crosslinkable chemical end-groups either at one or both ends of the mesogen (Figure 5a), were first developed in the 1980s.[97] A selection of common materials and their names

are given in Figure 5b. By reacting the crosslinkable chemical groups, the RMs are chemically bonded, fixing the mesogenic alignment pattern (Figure 5c). This densely crosslinked material is known as an LCN. LCNs characteristically have glass transition temperatures (T_g) above RT and high crosslink densities.[86]

Reducing the crosslink density can be accomplished by forming LC oligomers by chemically concatenating RMs before crosslinking: the experimental procedure is detailed in Section 4.2. Crosslinking LC oligomers leads to a loose network, known as an LCE, which are as the name suggests, more "elastic"; they typically feature viscoelastic, non-Newtonian flow behavior[34,76,98] with large strain-at-break values and low elastic moduli at RT compared to the densely crosslinked LCNs (Figure 5d).

2.2.3. Liquid Crystal-Based Actuators and Actuation Triggers

Molecular alignment coupled with chemical crosslinking is the basis of many "smart" applications, including 4D printing of LCs. The most basic actuation arising from planar and homeotropic crosslinked networks is thermal contraction, but many other, more complex motions are possible. With increased temperature, mesogens making up LC networks naturally lose order, the "order–disorder transition," which in the case of an aligned network leads to contraction along **n** as the mesogens pull the network together through their crosslinked ends, and expansion perpendicular to **n**. However, temperature is not the only stimulus available for generating this order–disorder transition. In the following sections, we will discuss both the variety of actuation possibilities and the variety of available triggers.

Actuation: Reduced crosslink densities, as found in LCEs, leads to large contractions, since the order–disorder transition is given more freedom to strain the network.[99] When it comes to designing a 4D printed object with LCEs, the two distinguishing features, freedom in structural design, and mesogen alignment, are best used in synergy. As depicted in **Figure 6**, the molecular alignment of the liquid crystals determines the direction of contraction and/or bending. For example, a strip with uniaxial molecular alignment leads to contraction along a single direction, a design suited for artificial muscles (Figure 6a). In cholesterics, since there is a continuously rotating molecular director distribution along the helix director, disorder leads to expansion along this helix director and a slight contraction in-plane.[100] Out-of-plane deformation, similar to the workings of a hinge, can be accomplished with molecular director patterns such as splay and twisted (see Figure 6b). Twisting actuation results from actuator with their long axis offset from **n**.[101] By more intricate patterning of the alignment, highly localized responses can be generated leading to functional actuation pathways.[102] Concentric and azimuthal alignment patterns can also result in out-of-plane actuations, as these concentrate stresses to a single point (Figure 6c).[103,104] Tiling multiple concentric domains together leads to the formation of multiple cones within a single film, which can be used to lift masses.[105,106]

The influence of the fabricated object's macroscopic shape has been demonstrated in thin-film LCN devices. Planar films produced with the length cut at angles oblique to **n** lead to coiling upon actuation.[101,107] In splay films, having **n** on the planar aligned side parallel to the film's long axis ("**n** ∥ film") forms a thin coil, while having "**n** ⊥ film" leads to tube formation (this does not hold for twisted alignments). To add variability, the degree of bending is inversely related to the film thickness, thereby serving as an additional design parameter;[108] by varying thickness along the film, in essence creating a wedge, the amplitude of the bending can be dramatically enhanced, resulting in tightly rolled films (Figure 6d).[108] Thus, it is not only the molecular alignment, but also the geometry that has a significant role in actuator performance. Normally, combining domains of different alignments within a single film requires intricate alignment procedures, so assemblies of multiple LCN films have been explored in preference (Figure 6e). Orienting films in an assembly where they bend toward each other has been used as grippers and feet.[109–112] A film with localized director patterns and cuts in strategic locations can lead to the reversible opening and closing of those cuts through actuating the LCN.[113] Combining an LCN with a support material in a bilayer fashion can also guide the film to bend or curl, akin to bimetallic strips.[114,115] For more information on different alignment-shape combinations, we refer the reader to reviews that showcase actuator designs and principles.[48,51]

Sections 3 and 4 demonstrate how additive manufacturing techniques make it possible to functionally combine free-form LC alignment patterns and shape design in devices or assemblies that were previously difficult or impossible to fabricate, leading to new applications for LC materials.

Triggering: Through development of different reactive mesogenic formulations, LC order–disorder transitions can be engineered to make materials that actuate in response to light (UV[86] and visible[116]), humidity,[101] chemical analytes,[117] and temperature;[34,118] additionally their interaction with light can be modulated.[119] In the following subsections, we briefly discuss how materials can be made sensitive to these different triggers: more specific examples of materials and techniques are presented in Sections 3 and 4 (**Figure 7** for common environmental responsivities).

Light Triggered Actuation: Light responsivity in LCNs is typically obtained by including a dopant in the host LC network that either generates local heating (a photothermal effect), or changes its conformation (a photomechanical effect) on light exposure.[120,121] Both mechanisms appeal to different applications.

In a photothermal effect, the dopant absorbs light and subsequently releases the energy, increasing the local temperature of the network, generating a physical response. Upon removing the light source, the sample rapidly cools, and the response reverses. Different classes of dopants have been incorporated in LC mixtures without disturbing the alignment of the mesogens and granting the network of a photothermal response to different wavelengths. Monoacrylate-functionalized azobenzenes can be incorporated to give response to UV and visible lights.[121] Visible and near-infrared (NIR) light response has been achieved by incorporating gold nanoparticles,[68,122] carbon nanotubes (CNTs),[123] or graphene.[124] Typically, these dopants are incorporated at concentrations of 1–10 wt%.

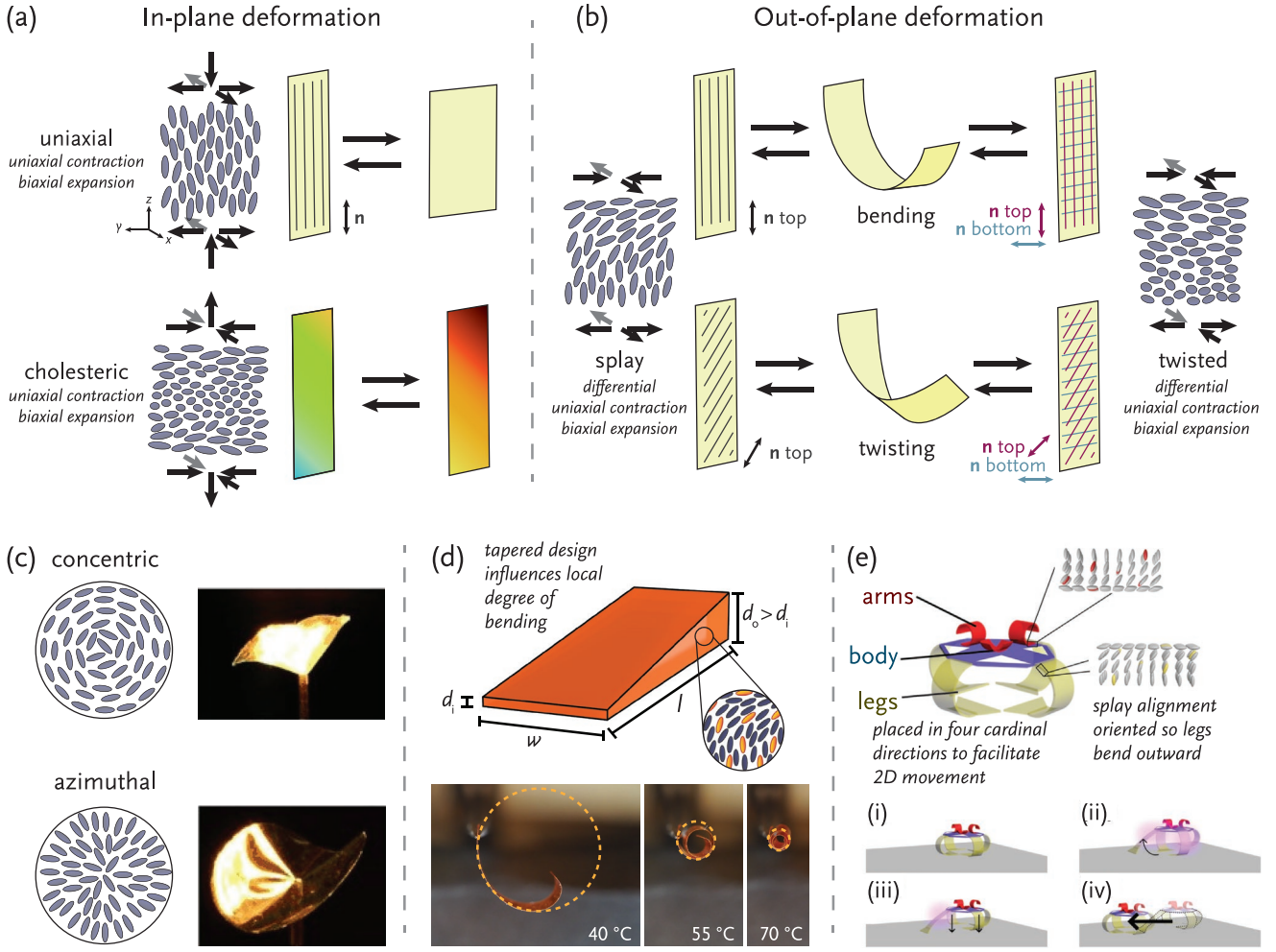

Figure 6. Contraction and expansion directions for different LC alignments in response to increased disorder: a) uniaxial, cholesteric, b) splay, twisted. c) Complex alignment patterns concentric and azimuthal depicted schematically and their response when crosslinked into an LCN. Adapted with permission.[104] Copyright 2012, Wiley-VCH. d) Schematic drawing of a tapered actuator design with photographs showing the obtained effect upon actuation. Adapted under the terms of the CC-BY Creative Commons Attribution 3.0 International license.[108] Copyright 2019, Royal Society of Chemistry. e) Example of an assembly of LCNs in which the alignments and orientations of different actuators have been chosen in such a way that 2D movement is possible. Steps (i–iv) illustrate the steps that make up a full "walking cycle": i) walker in its original location, ii) legs perpendicular to intended movement direction irradiated, leading these to bend outward and temporarily lift the robot, iii) front leg is triggered to bend forward, and finally iv) the leg retracts, pulling the walker into the intended direction. Adapted under the terms of the CC-BY Creative Commons Attribution 4.0 International license.[111] Copyright 2020, Wiley-VCH.

In the photomechanical response, the dopant changes its conformation upon absorbing light, forcing molecular rearrangements and triggering stress in the network. Difunctionalized acrylate azobenzene dyes, which are compatible with LCs, are common dopants for generating photomechanical molecular disorder.[51,60,106,125–127] Azobenzene-doped materials generally respond to both UV and blue lights (peak absorption wavelengths typically λ_{exc} = 365 nm for *trans*→*cis*, and 450 nm for *cis*→*trans* photoisomerization).[121] By photoisomerizing, the difunctional azobenzene molecules generate a photomechanical contraction of the network along the molecular director, which is transduced to the macroscopic object as a contractile strain.[51,86]

Additionally, if the light extinction caused by the absorbing photoswitch is strong enough, differential contraction between the isomerized and nonisomerized regions can occur, which can lead to a bending motion.[60,126] When the light source is removed, the deformation is maintained until the dopant responsible for generating the stresses returns to its initial state over time. This conformational change can have a lifetime varying from seconds to months,[116,128] so reversible, bi-stable responses can be achieved. Photomechanical responses have the advantage over photothermal responses underwater in that the actuation can be achieved at lower light intensities, since the photomechanical actuation mechanism is not dependent on heat generation, and thus, does not require an insulating medium (such as air) surrounding the actuator.

Humidity Triggered Actuation: Physical response to humidity can be integrated in the LC network by incorporating mesogens with hygroscopic groups which attract environmental moisture:

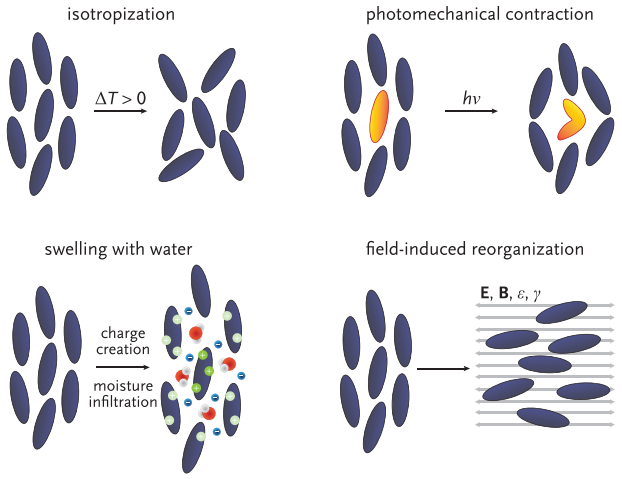

Figure 7. Idealized schematic drawings of molecular responses to four different stimuli: temperature (isotropization), photomechanical (photoisomers), swelling in response to water, and field-induced reorganization (typical examples **E**: electric, **B**: magnetic, ε: strain, γ: shear).

a controlled swelling of the network is achieved dependent on the volume of water taken up. Hydrophilic blocks[129] or polar groups[50,130] are incorporated to make the LC as a whole water-absorbing. Polar groups (carboxylic acids or tertiary amines) are not yet sensitive to humidity immediately after polymerization: to become active, these must be activated using alkaline or acidic aqueous solutions, respectively. Owing to the anisotropic character of the LC network, the resulting swelling upon water absorbance can also be anisotropic.[101,131]

Electrical/Magnetic Triggered Actuation: Besides orchestrating a molecular reorientation, electrical and magnetic fields can also be used to trigger thermal actuation. This can be done by loading the LC with a conductive liquid metal,[132–134] or by creating a bilayer of an LC film and an iron doped polydimethylsiloxane (PDMS) layer, where exposure to strong magnetic fields causes induction heating of the sample.[135,136] Addressing electrically or magnetically presents some advantages over other actuation schemes: the response is near-instantaneous and does not suffer from light attenuation as often happens in actuators relying on absorption of a dye.

3. Vat Polymerization for Stimuli-Responsive Micrometer Scale Objects

Fabrication of micrometer scale LC objects has been accomplished mainly via TPP-DLW, a favorite tool for researchers for producing microscale structures as it offers both sub-micrometer resolution and freedom of structural design compatible with a wide variety of photoresists.[137–141] Different LC mixtures and alignments can be employed, which allow for the fabrication of microstructures as diverse as microgrippers,[30] microlenses,[142] microwalkers[31] or different photonic elements.[32,63] In the following sections we will discuss: 1) the effects of the printing parameters on the final LCN network, 2) how to prepare and tune LC photoresists suitable for use in TPP-DLW, and 3) review some recent examples of LC microstructures enabled via TPP-DLW.

3.1. TPP-DLW Printing Parameters

There are several tunable printing parameters that not only influence a structure's fidelity to the computer design, but, in the case of TPP-DLW in LC photoresists, also affect the characteristics of the network formed, and even how the final print actuates (**Figure 8**).

3.1.1. Achieving Liquid Crystal Alignment

Controlling the alignment of the mesogens allows for the preprogramming of the response of the structures. In addition to the standard aligning techniques described in Section 2.2.1, the mesogens can be aligned by using a micropatterned glass plate,

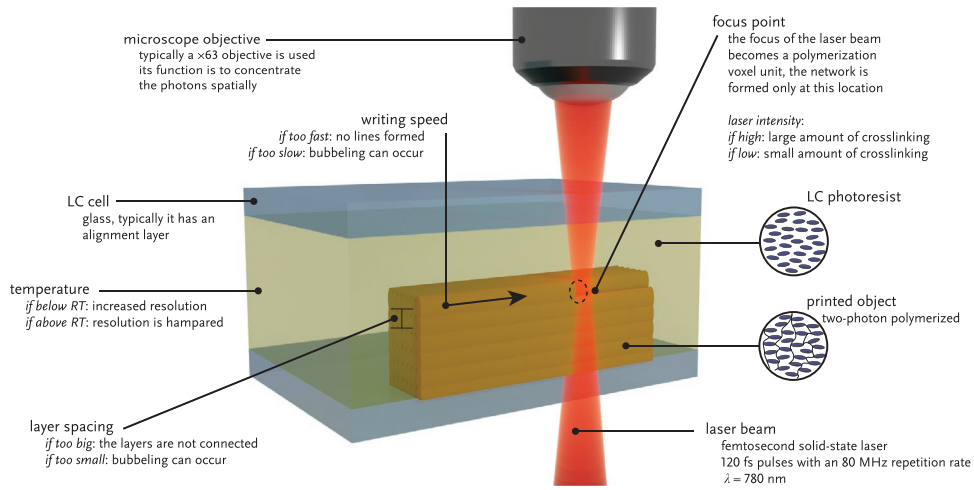

Figure 8. Schematic representation of the printing process of LCs in TPP-DLW. In the drawing, the different user-adjustable parameters are highlighted: the writing speed, laser intensity, temperature, and layer spacing. The insets for LC photoresist and LCN show an example for an approximate orientation of the mesogens, in this case planar, in the vat, and after polymerization, which are typically the same.

the topography of which provides the boundary conditions necessary for the molecules to align. This micropatterning can be either 2D[92,143,144] or 3D,[145–148] and may be fabricated using diverse techniques. Alignment of the LC molecules can be achieved with a microscopic resolution via TPP-DLW micropatterning, leading to variations in molecular order within the same microstructure, making programming different deformation modes within the same object possible.[33]

An intriguing possibility for induced molecular alignment during printing by tuning of both scanning speed and laser polarization was presented.[149] Unfortunately, confirmation of this finding has not been forthcoming, and it appears difficult to reproduce for other LC mixtures, and so has attracted little attention. Nevertheless, exploring a system which aligns along the printing path would increase control over the molecular alignment within structures and it would open new modes of deformation.

3.1.2. Layer Spacing and Infill

As stated in Section 2.1, there are two key choices to be made before printing the CAD design that have a direct influence on the network and structure: slicing and infill. When slicing, the distance between layers should not be larger than the size of the laser focal point: if the distance is too large, the layers will not be connected and so will float away during printing. If they just make contact, then connection between layers will be weak and the structure's performance is hampered. If they overlap too much, the temperature can be increased locally in the points were there has been already a network formed, which can lead to bubbles forming during printing. Hence, several different layer spacings are typically tested to determine the optimum. Usually, the more layers used to fabricate the CAD design, the higher the fidelity of the printed structure to the design. Thus, it is a matter of a compromise between the number of layers and the capability of maintaining enough space between them during printing to obtain structures most representative to the intended design. Note that printing is typically started with the laser focal point ≈0.5 µm into the substrate; this to ensure good adhesion of the structures with the substrate, which pre-empts delamination during the developing stage. As a result, the final structures are somewhat shorter than the CAD design. Additionally, when a too densely patterned infill is selected, undesirable bubbling can occur due to the laser point passing through previously polymerized polymer network.

Through careful selection of infill type, a sort of "skeleton" within the structure has been created that programmed a rotational motion within a hydrogel pillar.[150] This effect of using the infill to influence the structure performance has not yet been reported in LC structures, but it would be an interesting study.

3.1.3. Laser Power, Scanning Speed, and Temperature

During printing there are two main parameters that can be tuned: 1) the power and 2) the scanning speed of the laser, both directly affecting the quantity of polymerization initiation points formed and eventual crosslink density of the final print. Varying laser power increases or decreases the flux of photons at the focal point, while the scanning speed determines the photon dose at one location. Since TPA is all about probabilities, the longer a greater number of photons are incident at one location, the greater the probability for TPA to occur and so the more nucleation points and thus crosslinks form. Only in recent years has local modification of the crosslink density within the structure by changing the printing conditions during TPP-DLW "on the fly" been a hot topic.[151–154] This has been demonstrated in hydrogels, in which structures were fabricated using different laser powers and scanning speeds, resulting in clearly differentiated performances upon swelling.[151,152] For LC structures, similar effects have been reported,[63,155,156] but the consequences to the structure's performance have not yet been studied.

It has been recently shown that temperature also plays a role in the resolution achievable by an LC photoresist.[157] At temperatures below RT, diffusion of unreacted monomer into the polymerized network causing swelling is reduced, improving the resolution of the structure, while at elevated temperatures, above RT, swelling is enhanced, reducing resolution. This temperature effect is because diffusion of the monomer is a thermodynamic phenomenon, and as such, is temperature-dependent. As a result, temperature is an "easy" parameter one can tune to increase the microstructure's resolution.

3.2. Preparation of LC Photoresists for TPP-DLW

An LC photoresist for TPP-DLW must contain the following: 1) difunctional mesogens to act as crosslinkers to form the network and fix the alignment in place, 2) monofunctional mesogens to provide flexibility to the network, and 3) a two-photon photoinitiator. However, a fourth condition can be imposed by the TPP-DLW equipment: 4) the material must have a stable LC phase at RT when there is no heating stage. Most reported LC mixtures satisfy the first three requirements, but their LC phases typically exist above RT or crystallization at ambient conditions occurs after only a few minutes, reducing the available printing time, and hence making these mixtures generally unsuitable for printing. While actual printing times may vary, in our experience single micrometer scale structures require a few seconds to complete, while structures on the order of a few hundred micrometers take minutes. What usually takes the longest is the period between filling the LC alignment cell and the actual onset of printing, which can take half an hour. This latter restraint imposed by the equipment can be overcome, for example by custom stages allowing heating of the mixture during printing.[157,158]

Other factors are relevant when selecting the mesogens for the photoresist. In general, stimuli-responsive objects are typically based on low crosslink density materials, and as a result suffer from swelling with the surrounding monomer both during and after the TPP-DLW process,[150,159,160] reducing resolution. When working with LCs, swelling can be avoided by increasing crosslink density, that is, the fraction of mesogens with two reactive end groups, which in turn improves the resolution achievable with the resist. Nonetheless, when working

with acrylate-terminated monomers, increasing the fraction of bifunctional mesogens augments polymerization shrinkage. The use of epoxide and oxetane mesogens rather than acrylates can be used not only to reduce polymerization shrinkage, but also to ensure oxygen insensitivity during polymerization and a lower processing viscosity.[158,161] Despite their advantages, epoxide-based LCNs are still in their early stage when compared to acrylate-based LCNs.

The ratio of difunctional to monofunctional mesogens is an important parameter affecting the structure's resolution, but increasing the crosslink density degrades the performance of the actuating structures, as both speed and amplitude in actuation response are reduced.[160] This effect can be exploited to obtain nonreciprocal motion in microstructures that have regions composed of mixtures containing different ratios of difunctional to monofunctional mesogens, thus differing crosslink densities.[162]

Regarding two-photon photoinitiators, a wide variety are suitable for use in TPP-DLW.[163–165] The choice of initiator must consider the polymerization mechanism of the reactive groups of the mesogens. Most work with LCs has used acrylate-terminated mesogens, which conventionally work with a free radical generator to initiate polymerization. To this end, bis(2,4,6-trimethylbenzoyl)phenylphosphine oxide (**P1**)[59,93,94,149,156] or 2-benzyl-2-dimethylamino-1-(4-morpholinophenyl)-butan-1-one (**P2**)[30,31,68,157,159,160,166–168] have been used in TPP-DLW (Figure 5; Table S2, Supporting Information). Of these two, **P2** has a higher TPA,[165] so polymerization can be achieved at lower laser power and at faster scanning speeds. On the other hand, there are also examples of epoxide and oxetane-terminated mesogens, which instead require a cationic photoinitiator to induce the ring opening polymerization. In the case of epoxide-terminated mesogens, H-Nu-470 (5,7-diiodo-3-butoxy-6-fluorone) and H-Nu-254 (an iodonium salt derivative) at a ratio of 15:1 w/w have been successfully used for TPP-DLW.[158]

3.2.1. Standard LC Photoresist for TPP-DLW

An example LC photoresist that satisfies all the conditions presented in Section 3.2 that allows production of microstructures with optimal responses with a resolution up to 160 nm is composed of 30 mol% LC diacrylate **R1**, 69 mol% LC monoacrylate **R3**, and 1 mol% free radical photoinitiator **P2**.[160,166,169,170] This mixture is nematic from RT to ≈60 °C; crystallization at RT only occurs after several hours. By using different boundary conditions in the LC alignment cell, both planar and splay alignments can be achieved. After polymerization, the network shows a temperature response, contracting up to 20% along molecular director **n**.[31,68,162,167]

3.2.2. Augmenting the Standard LC Photoresist with Additional Functionalities

Adding dopants to an LC photoresist may allow integration of additional optical properties, functionalities and/or improve the mechanical performance of the network (Section 2.2.3). The two most important considerations when choosing a dopant are: 1) it should not disturb the molecular alignment and 2) it should be transparent to the laser light, or at least not compete with TPA. The former can be easily satisfied by choosing a dopant that has dimensions and shape like the rod-like LC mesogens, while the latter is more specific to the material and chemical groups possibly present in any dopants. An overview of sample LC photoresists is given in **Table 1** and in **Figure 9**.

Light Response: UV–vis light response is typically obtained by incorporating azobenzene chromophores into the LCN (Section 2.2.3). However, azobenzene dyes generally have absorption tails around 400 nm from the *trans*-isomer, so incorporation of these dopants can be challenging: commercial TPP-DLW equipment uses $\lambda = 790$ nm lasers, resulting in TPA at $\lambda = 395$ nm, meaning the azobenzene is liable to absorb this laser light, which can lead to both bubble formation due to sudden heating at the focal point, and/or slowing polymerization due to spectral overlap with the absorption peak of the photoinitiators. Both effects can be avoided by changing the substituents on the azobenzene to red shift the absorption from $\lambda = 350$ nm to around $\lambda = 530$ nm.[159] Using such a dye (**L1**), several examples of microstructures responsive to green light have been reported.[30,31,168,169]

Recently, the possibility of fabricating microstructures responsive to NIR light has attracted attention. NIR offers a

Table 1. Overview of reported LC photoresists used in TPP-DLW equipment.

Mesogens	Ratio	Additive	Network responds to:	Refs.
R3:R2	66:33[a)]	N/A	Temperature	[33,171]
	90:10[b)]	1–3 wt% Au NRs	NIR light[c)]	[68]
	68:30[b)]	1 mol% L1	Green light[c)]	[157,160,166,169,170]
	78:20[b)]			[30,31,159]
E7 mixture:R2	70.7:28.5[a)]	N/A	Electric field[d)]	[32,95]
	68.5:26.8[a)]	4.1 wt% chiral dopant		[93]
R1-2:R3-4:W1–4[e)]	6.5: 23.4:67.1[b)]	2.3 mol% C2	Humidity	[59]
Epoxide-terminated LC[f)]	100[b)]	N/A	Temperature	[158]

[a)]Weight-based ratio; [b)]Mol-based ratio; [c)]Response based on a photothermal effect; the dopant allows for a remote control of the structures' temperature; [d)]The monomers (not the network) respond to the electric field; [e)]**R1-2** are diacrylate mesogens, **R3-4** are monoacrylate mesogens and **W1-4** stands for monofunctional mesogenic carboxylic acids mesogens, **L1** and **C2** stands for monoacrylate azobenzene and chiral dopant respectively; see Figures 5 and 9 for their chemical structures; [f)]Different diepoxide-terminated mesogens are evaluated.

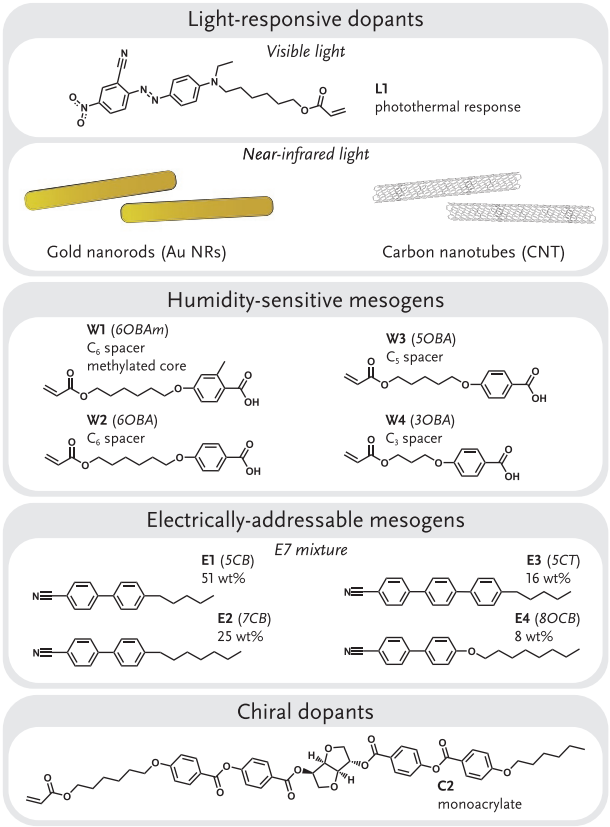

Figure 9. Overview of most common dopants used to grant responsivity to the network used in TPP-DLW. In parenthesis are the commercial names of the molecules. Full names are given in Table S4 in the Supporting Information. Synthetic protocols for **L1** and **C2** can be seen, repectively, in ref. [159] and in ref. [172].

less energetic trigger with greater penetration depth in biological tissue, and causes less damage than UV light, so potentially important for in vivo actuator designs.[173] Gold nanorods (Au NRs) have been used to facilitate a NIR response in TPP-DLW generated LC microstructures.[68] Owing to their shape, Au NRs can be incorporated in the LC network without disturbing alignment. Despite the Au NRs absorbing 790 nm laser light, bubbling was avoided by printing at lower laser powers. The addition of 3 wt% Au NRs not only granted the network NIR response, but also improved mechanical properties by almost doubling the storage modulus.[68] While graphene proved an unsuitable replacement for Au NRs due to its high absorbance at $\lambda = 790$ nm, CNTs allowed polymerization without bubbling despite also absorbing in this range.[174] However, photoresists doped with Au NRs have a lower polymerization threshold than photoresists containing CNTs so the former remains a more attractive dopant for imbuing responsivity to NIR light.

Humidity Response: Response to humidity is typically obtained by the incorporation reactive hydrogen bonded carboxylic acid dimers into the LCN (Section 2.2.3). The addition of these dimers to the photoresist for TPP-DLW has both advantages and disadvantages. The molecules act as supramolecular crosslinkers, so during TPP-DLW there is a high crosslink density: both chemical and supramolecular bonds. This reduces structural swelling with monomer during printing. Postfabrication, the base treatment cleaving the supramolecular bonds reversibly reduces the crosslink density without significantly affecting the structure's overall shape, granting the network the capability of larger actuations. However, monofunctional mesogenic carboxylic acids typically have relatively high melting points, and RT LC phases are rare,[59,175] which often precludes their use with commercial TPP-DLW systems that do not have heating stages. RT LC phases are possible in complex mixtures combining multiple distinct mesogens.[59]

Electrical Response: To obtain electrically addressable LC mixtures, mesogens having strong dipole moments are required in the photoresist (Section 2.2.3). The commercial LC mixture "**E7**," Figure 9, has been extensively used in LC research to prepare mixtures that can be addressed via an electric field.[176–178] The **E7** mixture is liquid crystalline at RT and thus suitable to use in TPP-DLW equipment. **E7** is composed of nonreactive mesogens, so to form a network reactive mesogens need to be added. A mixture with the diacrylate **R2** at ≈27 wt% and ≈73 wt% **E7** has been shown to have an LC phase stable for several hours at RT and be suitable for producing microstructures via TPP-DLW.[32,93,95] While this mixture results in a network, it is not suitable for the fabrication of freestanding objects, since during the developing step the unreacted **E7** is washed away, leaving the network with pores and a susceptibility to collapse. To produce mixtures that can form free-standing structures addressable with electric fields, a reactive mesogen that has a large dipole moment, like **R4**, is preferred. There is one reported mixture that contains the monoacrylate **R4** that has been used in TPP-DLW equipment,[59] although the electrical addressability of the mixture was not explored.

Structural Color: As discussed in Section 2.2.1, a chiral dopant induces a helical arrangement of LC molecules and results in a photonic 1D pseudo-Bragg reflector.[52] Upon triggering the response, the reflected color by the network shifts, typically toward longer wavelengths. This shift is accompanied, or induced, by the expansion/contraction of the network, see Equation (4). When fabricating photonic structures at the micrometer scale, one needs to recall that the thickness of the structure needs to be at least ten times the thickness of the pitch for it to produce visible reflected color.[59]

3.3. 4D Printed Micrometer Scale LC Structures

Using TPP-DLW, a wide variety of LC microstructures has been fabricated (**Table 2**). These can be classified in groups according to different criteria, e.g. trigger of the response, application, properties, etc. In this work, we choose to categorize them in two different groups according to the structure's intended purpose. Thus, structures that have shown to interact with light, either because of their molecular arrangement or due to their dimensions, are grouped as photonic microstructures (Section 3.3.1); structures that show a shape deformation triggered by an external stimulus are grouped as microactuators (Section 3.3.2). As a result, some structures that could be considered microactuators are grouped with photonic structures since they use the anisotropic shape of the network to obtain dynamic optical properties.

Table 2. Overview of the different microstructures enabled via TPP-DLW.

Type of device	Method to align the mesogens	Alignment configuration	The network responds to	Refs.
Gripper	Alignment layer	Splay	Light[b)]	[30]
Walker		Planar		[31]
Periodic structures[a)]				[166,169,170]
Resonators				[167]
Anti-counterfeit features	Electric field	Planar, tilted, homeotropic	Temperature[c)]	[32]
	Alignment layer	Planar	Temperature	[171]
Reflective structures	Self-assembled	Cholesteric	Temperature	[63,155,179,183]
			Light	[156]
			Humidity	[59]
Nature-like structures[d)]				
Lenses	Micropatterning	Controlled localized rotation of the molecules	Temperature[c)]	[142]
Various 3D geometries	Electric field	Planar, tilted, homeotropic	Temperature[c)]	[94]
	Alignment layer	Planar	Light[b)]	[68]
	Micropatterning	Controlled localized rotation of the molecules	Solvent	[33]
Patterns	Alignment layer	Planar	Temperature	[158]

[a)]Owing to their small periodic features, these structures modulate light; [b)]In this example, light is used to remotely control the structure's temperature, which triggers the response; [c)]In this example, the network does not show a shape change due to temperature, but it changes its refractive index; [d)]For nature-like structures, we understand butterflies, flowers and so on.

3.3.1. Photonic Microstructures

A microstructure is considered photonic when it interacts with light, mainly through reflection and diffraction in printed materials. This can occur at two different length scales: the molecular level when the light is modulated by chromophores in the material itself, and/or the nanometer to micrometer scale when light interacts via the geometry and periodicity of the structural features. Owing to the optical anisotropy of LCs, it is possible to fabricate photonic microstructures that interact with light simultaneously at different length scales.

The first LC photonic microstructures were generated via TPP-DLW in 2006.[179] As described in Section 2.2.1, mesogens can be self-organized in a helical fashion that results in a 1D photonic crystal, constituting a photonic polymer. This comes with the advantage that physical shape of the print can be chosen arbitrarily. This early work focused on studying defect modes in cholesteric networks by polymerizing part of the top and bottom of the cell while leaving the intermediate region with unreacted monomers; in essence creating a polymer–monomer–polymer sandwich. After polymerization, the pitch length elongated by a factor of 20% in the polymerized regions, while the pitch length in the unreacted regions was reduced. The contrast between the center of the selective reflection band (SRB) between the polymerized and the unreacted regions resulted in a stable single-defect mode sensitive to temperature, resulting in a reflection band red shift of 36 nm upon heating the sample by 30 °C. Further investigation of the potential of this chiral molecule diffusion was explored by fabricating frames with microscopic indentation which allowed a fine control of the shift of the SRB (**Figure 10**a).[180] These photonic microstructures have the potential to become stimuli-responsive narrow bandpass filters, heat sensors in integrated optical circuits, or/and advanced optical and photonic components.

The cholesteric alignment can also be used to fabricate photonic microactuators (Figure 10b).[59] The controlled expansion/contraction of the microstructures results in a controlled change of the helical pitch that in turns affects the reflected color. Since both the photonic response and the shape change are connected (Equation (4)), the former can be used as an intrinsic probe for the latter. This synergetic change of the structure's color linked to the expansion of the network could be beneficial in microelectromechanical systems (MEMS) or in microrobots to enhance their tracking in real-time,[181] which is much desired in the micro realm, due to the difficult readability of the structures.

Instead of making use of the cholesteric alignment to fabricate structures in which the materials themselves interact with light, the inherent birefringence of the LC can also be used (Section 2.2). When combining electrically addressable LC photoresists with TPP-DLW, the molecular alignment during fabrication can be easily controlled and tuned.[32,93–95] Hence, during fabrication, different molecular alignments can be fixed. As a result, one can accomplish complex spatial variations on the birefringence inside the cell, as the polymerized regions and the surrounding monomer can have different molecular alignments.[94] When that is the case, the optical mismatch results in scattering and the structures being visible; but when viewed under an applied electrical potential matching the potential used during polymerization, the polymerized and nonpolymerized components match in birefringence, and the structures become indiscernible (Figure 10c).[32] Alternatively, the birefringence of LC microstructures can also be used to fabricate temperature-responsive color pixels for

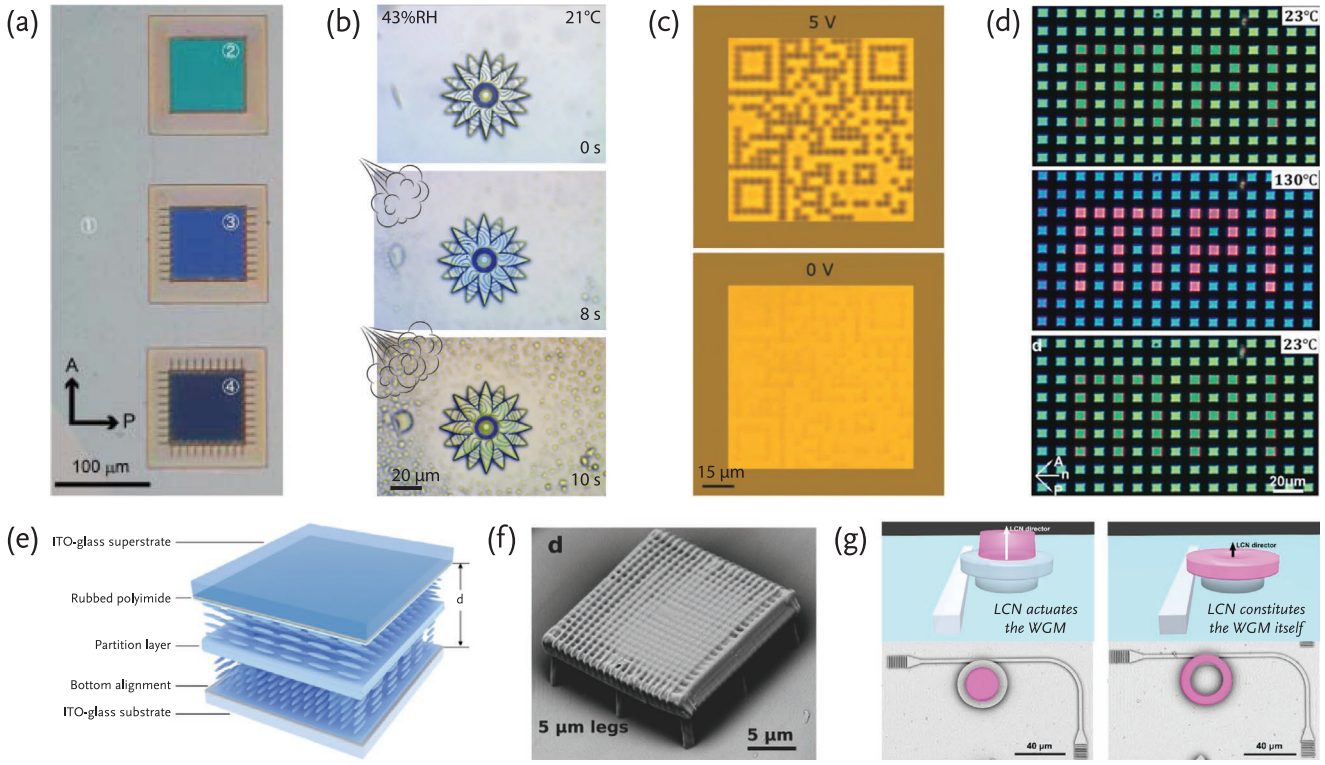

Figure 10. a) Polarized optical micrograph (POM) images of three CLC structures in which the SRB is controlled by introducing indentation in the frames; top without indentations, middle with 20 slits and bottom with 40 slits. Reproduced with permission.[180] Copyright 2008, Optical Society of America. b) A sequence of micrograph showing the response of a photonic microactuator, in this case a flower, to breath. Adapted under the terms of the CC-BY Creative Commons Attribution 4.0 International license.[59] Copyright 2020, American Chemical Society. c) POM images of a quick-response (QR) code formed by micropillars that were polymerized when no electrical potential was applied and consequently the QR code is only visible when a potential is applied. Adapted under the terms of the CC-BY Creative Commons Attribution 4.0 International license.[32] Copyright 2018, Wiley-VCH. d) POM images of arrays of pillars presenting different highs. As a result of the height difference, an encoded message is visible upon heating the structures. Adapted under the terms of the CC-BY Creative Commons Attribution 4.0 International license.[171] Copyright 2020, Wiley-VCH. e) Schematic of a polarization-independent phase modulator that consist a 3D scaffold that align the mesogens in distinctly along the structure. Reproduced with permission.[182] Copyright 2017, Optical Society of America. f) Scanning electron microscopy (SEM) image of a light-responsive diffraction grating having legs of 5 µm. Reproduced with permission.[166] Copyright 2012, Wiley-VCH. g) Two strategies to accomplish tunability on WGM resonator using LCN: on the left by placing a LCN on top of the WGM to actuate it and on the right by making the WGM out of LCN. On the top a rendered image depicting the strategy and on the bottom an SEM in which the LCN has been colored pink. Adapted with permission.[167] Copyright 2018, American Chemical Society.

encryption, encoding and anticounterfeiting elements at the microscale (Figure 10d).[171]

Another option using the birefringence of LC is making photonic microstructures via TPP-DLW micropatterns[92,145] and scaffolds[148,182] which serve to precisely change the director of the molecules within the structure. This 2D or 3D change in the arrangement of the molecules results in changes in the optical properties along the microstructure. As light travels through the network, the controlled change on the refractive indices can result in, for example, microlenses that specifically focus right-handed circularly polarized light and defocus left-handed circular polarized light, or vice versa,[145] or as polarization-independent phase modulators (Figure 10e).[182] Birefringence effects in microscale objects are rare and it would be of interest to investigate with LCs as starting point, as LC are well known for their use in LCDs which make use of their birefringence.

On the other hand, rather than using the internal material structure itself to interact with light, photonic interactions can be generated by fabricating periodic microstructures. Depending on the scale of the periodicity, the incident beam will be modulated or not. For example, gratings are well-known 2D photonic crystals that diffract incident light. When such a grating is made of a light-responsive LCN with a pitch of 1.5 µm (Figure 10f), it diffracts red light.[166] Owing to the anisotropic shape change of the LCN, the diffraction pattern could be altered by illuminating the grating with a green laser. The rapid response of the network resulted in the possibility of converting the simple static grating into a beam steerer.[166] Another example is to fabricate arrays of lines with a fixed width of 500 nm and a periodicity of 1.5 µm, with varying thicknesses between 250 to 750 nm.[169] Here, the polarization of the incident beam was changed during diffraction, not only due to the periodic change of the refractive index (polymer/air), but also because the grating was birefringent. The light-driven actuation changed both the shape and the optical character of the lines, which made it possible to dynamically control the polarizations of the diffracted beams, obtaining a nontrivial polarization transformation from a linearly polarized incident beam into three diffracted beams, two with an elliptical polarization states and one with a tilted state.

Finally, components for photonic circuits can also be made or controlled using LCNs, such as tunable whispering gallery mode (WGM) resonators,[168] which are microcavities with ultranarrow optical resonance. Since the cavity's functionality relies on the shift of the resonance frequency, WGM microcavities are attractive as optical sensors.[184] When the waveguide itself was partially made of LCN, the WGM resonance was blue shifted upon illumination (Figure 10g).[167] In contrast, if the WGM was instead made of a nonresponsive material and coupled to an LCN which was then actuated, the shape of the passive WGM changed, and red shifted the resonance. The LC-based WGM microresonator may also be made temperature-responsive.[185]

3.3.2. Microactuators

The key feature of microactuators is that there is a triggered shape change upon exposure to an external stimulus. LCs allow for the fabrication of microactuators that show a wide variety of preprogrammed shape deformations triggered by external stimuli. In this section, we will discuss the different examples of LC microactuators grouped by the stimulus that triggers their response.

LCNs are inherently responsive to temperature changes (Section 2.2.3); however, most of the work on LC-based microactuators has not focused on characterizing their response to this stimulus. This could be because it is difficult to analyze this response in microstructures and it is challenging to induce a controlled temperature change in only a single micro-object. Nevertheless, there is one example consisting of a hybrid system: LCN films that have embedded and epoxide-based micropatterns.[158] The epoxide-based micropatterns are first produced via TPP-DLW inside a cell, after which the nonreacted epoxide mesogens are removed and substituted by acrylate-functionalized mesogens that are used to then polymerize a film around the epoxide-based micropattern. The advantage of having a micropattern of a different material in the film comes from the enhanced mechanical and actuation performance of the composite which can be tuned by changing the geometry and dimensions of the patterns.

The first LC-based light-triggered microstructure, a microwalker formed by a body of planar aligned LC with four conical legs of a commercial, isotropic acrylate resin ("IP-Dip"), was produced in 2015 (**Figure 11**a).[31] Upon illumination with a λ = 532 nm (green) laser, the body contracted anisotropically, and when the light was turned off, it expanded to its initial state. Due to the rapid response of the body to a pulsed laser beam, the object could walk. Later work reported an autonomous light-responsive microhand composed of two strips forming a cross, each having splay alignment (Figure 11b).[30] Upon illumination, the strips bent, closing the hand. Again, when the light was turned off, the hand recovered its initial state. Autonomous motion was achieved, as light would be redirected by an object passing in front of the hand, triggering the response, and allowing the hand to catch objects by itself. More recently, there have been reports of 3D planar samples expanding anisotropically upon illumination with NIR light (Figure 11c).[68] In all these light-responsive microactuators, both to green and NIR light, the actuations were based on photothermal effects. Photomechanical actuation in LC-based microactuators has yet to be reported, but it would be more desired than photothermal actuation in some applications (Section 2.2.3), so worth exploring.

Response to ambient changes such as humidity and temperature, or to solvents, can also be desirable. In these cases, the response comes from the swelling of the network, expanding perpendicularly to the molecular alignment. This anisotropic swelling has been explored in microstructures that present different molecular alignments in the same geometrical object shape (Figure 11d).[33,92] As a result, different deformation modes triggered by swelling in *N*,*N*-dimethylformamide (DMF) could be obtained depending on the LC alignment. The solvent triggered an abrupt actuation, while humidity changes, in contrast, resulted in a gradual actuation, as has been shown in cholesteric microactuators (Figure 10b). Upon a controlled variation of the humidity the structures showed a reversible and controlled expansion/contraction perpendicular to the substrate.[59]

4. 3D Microextrusion for Stimuli-Responsive Millimeter to Centimeter-Scale Devices

Macroscale 4D printing of LCs is mostly performed using extrusion-based techniques, DIW in specific. Unlike techniques where the resin is in a bath (TPP-DLW, DLP), extrusion requires material that does not escape the nozzle under the force of gravity, yet flows well from an extrusion slot under pressure, and shows good setting behavior once on the substrate.[186] Such viscoelastic properties are found in oligomeric LCE precursors. The last few years of extrusion-based AM of LCs has catapulted one specific class of LCE precursor to the foreground of research: main-chain liquid crystal elastomers (MCLCEs), which are commonly synthesized from oligomers of concatenated reactive mesogens. MCLCEs maintain the anisotropic LC characteristics of the original monomers, but also are viscoelastic; their shear thinning behavior is what makes them useful for DIW. Here we will discuss: 1) the influence of the DIW printing parameters; their effects on the molecular alignment and on the final LCE object, 2) how to prepare and tune an MCLCE suitable for use in DIW, and 3) review recent examples of LCE devices enabled via DIW.

4.1. Direct Ink Writing Printing Parameters

After loading the ink reservoir with an LC ink composed of MCLCE and a suitable photoinitiator, printing can commence (**Figure 12**). The key variables that can be adjusted for DIW are printing infill, nozzle diameter, and printing temperature and speed, all of which influence the molecular order obtained after deposition, and thus device functionality. In the following sections, the influence of changing each of these printing parameters will be briefly discussed.

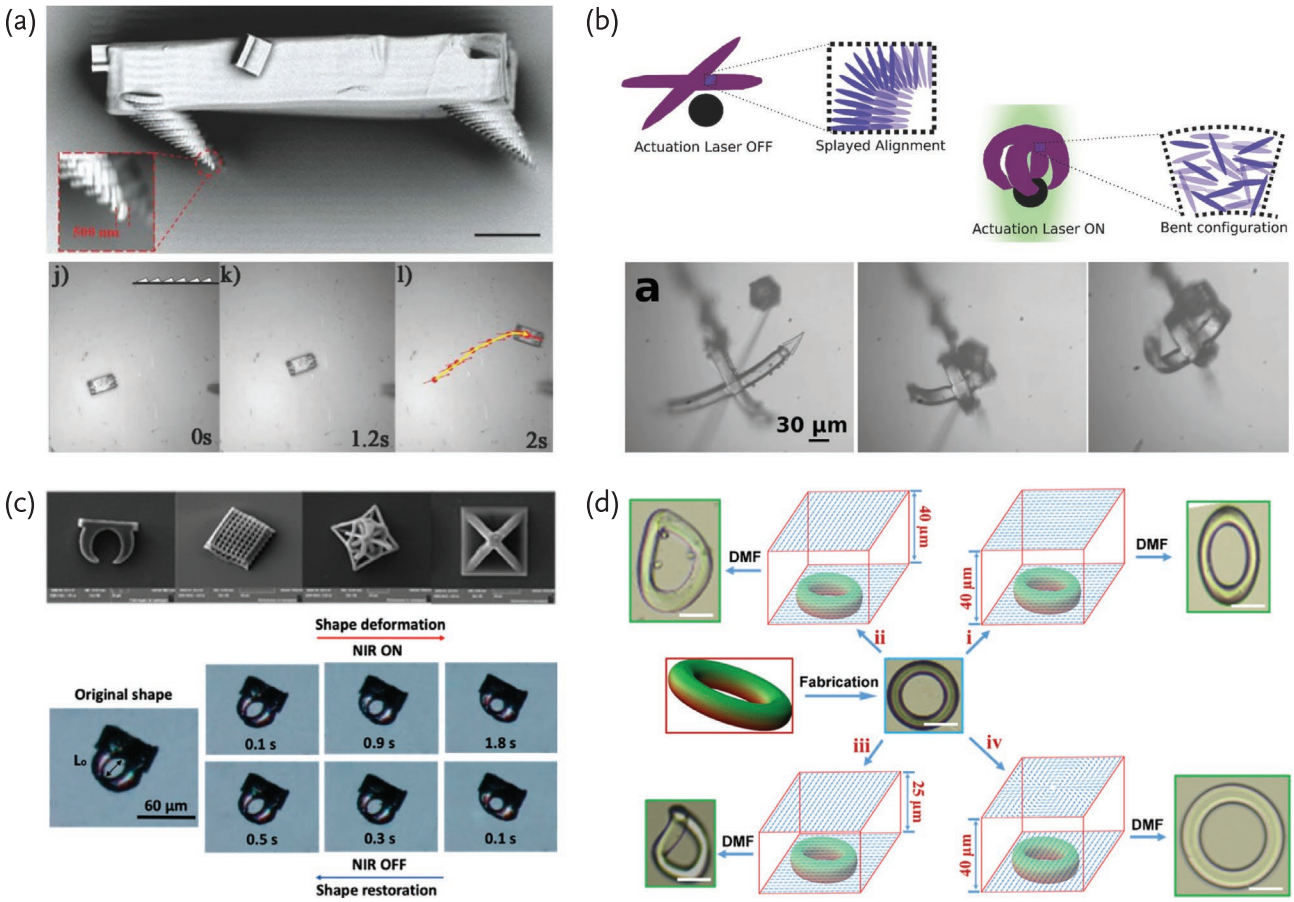

Figure 11. a) A light-fueled microwalker. Top: SEM image of the walker, scale bar 50 µm. Bottom: micrograph sequence that shows the walker movement upon illumination with a green laser. The topography of the surface is shown on the top left of the sequence. Adapted with permission.[31] Copyright 2015, Wiley-VCH. b) An autonomous light-responsive gripper. On the top, a scheme showing the mechanism for the response to grasp an object. On the bottom, micrographs showing the microhand in action. Adapted with permission.[30] Copyright 2017, Wiley-VCH. c) NIR light-responsive microstructures. On the top, SEM images showing diverse 3D geometries. On the bottom, micrograph images showing the response of structures to NIR light. Adapted with permission.[68] Copyright 2019, American Chemical Society. d) Various 3D-to-3D shape deformation from the same geometry, in this case a ring. The distinct deformations are accomplished by fixing different molecular alignment in the ring. Scale bars represent 50 µm. Reproduced under the terms of the Creative Commons CC BY license.[33] Copyright 2020, Wiley-VCH.

4.1.1. Infill Pattern and Nozzle Diameter

The most influential on the functionality of the final printed device is the infill, since typically the molecular alignment is parallel to the printing direction. As a result, the infill pattern decides how the object folds, twists, or bends after polymerizing the network. Examples of what can be expected from different combinations of alignments have been extensively reported (Section 4.3.1).[34–36,58,61,76,98,187–190]

The effect of the nozzle diameter has not been studied in detail, but it has been reported that smaller nozzle diameters lead to better uniaxial orientation of the mesogens in the deposited LC oligomer ink[190] while larger nozzle diameters lead to diminished molecular order.[76] Typical nozzle diameters used are in the 150–350 µm range, with typical layer heights being between 75–190 µm.[34–36,58,60,76,126] However, reducing the nozzle diameter increases the force needed to extrude the material and so depending on the equipment or the viscosity of the ink, some diameters are not suitable.

4.1.2. Printing Temperature and Speed

The surest way to getting good molecular alignment is by printing from the nematic phase onto a printing substrate that is at a lower temperature (RT is easiest).[34,36,76] The LC oligomer ink reservoir is generally heated to about 10–20 °C below the nematic to isotropic transition temperature (T_{NI}) for the best balance between molecular alignment after printing and "extrudability;" while possible to extrude the LC ink at lower temperature, it requires significantly higher extrusion pressures. Inks with low T_{NI}s (≈20 °C) have been printed successfully at RT.[187]

The thermal gradient from ink container to substrate also influences the molecular order in the final object.[190] With an increase of syringe temperature comes increasing disorder in the LC ink, recognizable as increasing opacity of the printed object, indicative of the formation of local, rather than uniform, alignment in the LCE ("polydomain alignment"). Opaque films do not show large actuation strains because of their low degree

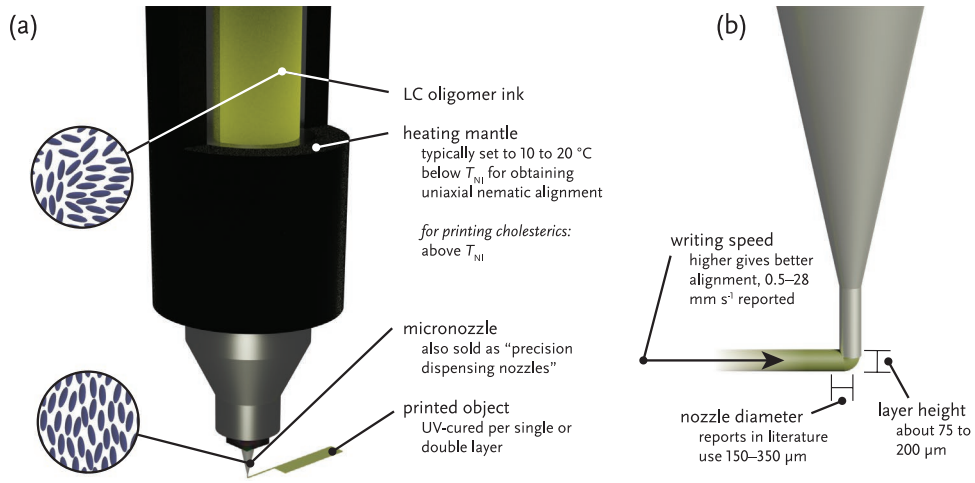

Figure 12. a) Schematic representation of the printing process, detailing the ink reservoir, nozzle, and printed object. The insets for "LC oligomer ink" and "micronozzle" show the approximate orientation of the mesogens in the reservoir, where it is polydomain nematic, and in the high shear environment of the micronozzle, where is it monodomain nematic. b) Detail schematic representation of the micronozzle showing user-changeable parameters: the writing speed, nozzle diameter and layer height.

of macroscopic molecular order. The temperature profile from ink cartridge to substrate can be engineered so that, combined with photoinduced crosslinking immediately after deposition, isotropic core–nematic shell orientations in printed LCE lines can be formed.[190] As a result of the temperature gradient in the deposited line, an outside layer of ordered uniaxial alignment forms, while the greater temperature deeper inside the filament allows for reorientation into a disordered polydomain state. The thinner the outer shell, the less the contractile actuation strain achieved upon subsequent temperature increase.

Printing speeds used for uniaxial nematic alignment are generally in the millimeter to centimeter per second range, with values in the range 0.5–28 mm s^{-1} having been reported.[34,36,58,60,76,98,126] Generally, higher printing speeds lead to better molecular alignment.[126,190] By depositing the LC ink at different speeds, controlled molecular order can be induced in the material, as a result of the stronger shear and elongational flow conditions at higher printing speeds.[188] This can be used as a design parameter: by varying the printing speed throughout the design, a single material can show local molecular order differences and be used to create different degrees of actuation across the sample during thermal contraction or solvent swelling, for instance.[188]

When printing LC phases that are not uniaxial, such as chiral nematic, it is not about maximizing the molecular order through shear flow, but by creating the proper conditions for the material to be deposited without inducing contradictory alignments. Chiral nematic LCs tend to self-align into the cholesteric phase, so by printing from the isotropic phase, with the ink reservoir above T_{NI}, very little uniaxial molecular alignment is organized during extrusion of the ink. The substrate is also heated, albeit below T_{NI}, to lower viscosity of the resin and allow for formation of the cholesteric phase. To help form a planar cholesteric alignment, low print speeds are used, in the order of 1–2 mm s^{-1}.[64] The appearance of the photonic prints can be modulated by further increasing the print speed.

4.2. Synthesizing an LC Ink for Direct Ink Writing

Two similar synthetic techniques have found wide appeal for making MCLCEs: amine-acrylate "aza-Michael" and thiol-acrylate "thiol-Michael" addition reactions (**Figure 13**).[191,192] Both techniques have been used extensively for linking diacrylate mesogens with chain extension molecules, the difference between aza-Michael and thiol-Michael being the reactant used for the chain extension. For amine-acrylate, the reaction is between a primary amine and a diacrylate and forms β-aminoester bonds between the reactive mesogens. Thiol-acrylate reactions on the other hand, form β-thioesters (Figure 13a).

When the diacrylate mesogen is in molar excess over the chain extender, the MCLCE mix obtained is acrylate-terminated (see Figure 13b) and can be photo-crosslinked after addition of a suitable free radical photoinitiator (Section 2.2.2). By photopolymerizing an aligned LC phase, for instance after mechanical stretching or directly after printing, a macroscopically aligned rubber is obtained that responds to temperature by contracting along the molecular director.[99,193] The strong thermal contraction seen in MCLCEs is based in the order to disorder transition around T_{NI} of the network, as the orientation of the aligned mesogenic cores randomizes and the network contracts in the direction of **n** (Section 2.2.3). In LCNs, contractile strains are generally below 10%,[54] being restricted by the high crosslinking density; in crosslinked LCEs, values up to 50% are common.

4.2.1. Making a Basic LC Ink

By virtue of the chemistry commonly employed, amine-acrylate or thiol-acrylate, the synthetic procedure for making the LC ink is fast and easily performed. Some of the first LCE printing papers even mention initiating the ink synthesis in bulk in the printer cartridge itself at elevated temperature.[36]

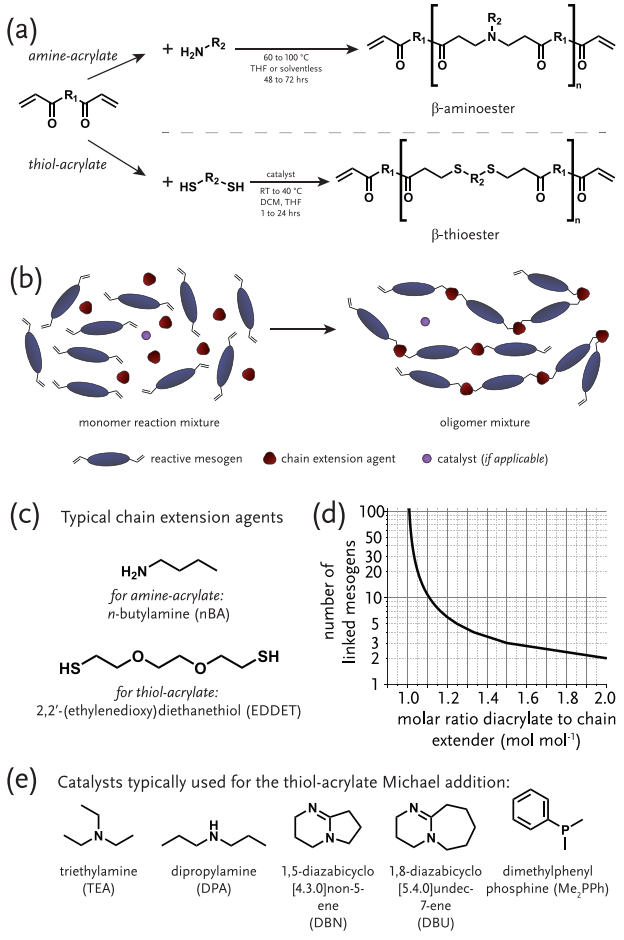

Figure 13. a) Schematic representation of the two common reactions used for making LC oligomers: amine-acrylate (aza-Michael) and thiol-acrylate (thiol-Michael). b) Schematic representation of the conversion of reactive mesogens to oligomers. c) Two common chain extension agents often used in the literature for the two different reaction schemes. d) Plot showing how the molar ratio "diacrylate to chain extension agent" influences the average length of oligomers formed. e) Common catalysts used for the thiol-acrylate reaction (Table S7, Supporting Information). Reaction rates[194] can be seen.

First, one must decide the desired chain length (in terms of mesogenic units). As the reaction is an addition polymerization, the resulting average chain length depends mainly on the reactant stoichiometry. For acrylate-terminated oligomers, the molar ratio of diacrylate to bifunctional chain extender ($\frac{n_{\text{diacrylate}}}{n_{\text{extender}}}$) needed for a "number-average LC units per oligomer" $\overline{x}_{\text{LC}}$ is

$$\frac{n_{\text{diacrylate}}}{n_{\text{extender}}} = \frac{\overline{x}_{\text{LC}}}{\overline{x}_{\text{LC}} - 1} \tag{6}$$

A typical LCE oligomer ink is designed around having an $\overline{x}_{\text{LC}}$ of 10, which, following from Equation (6), requires a molar ratio of 1.11 eq diacrylate to 1 eq chain extender (Figure 13d).[76] The chain extender can be a primary amine, such as *n*-butylamine, or a dithiol species, such as 2,2′-(ethylenedioxy)diethanethiol (Figure 13c). Typical reactive mesogens used for preparing an LC oligomer ink are **R1** and **R2** (Figure 5; Table S1, Supporting Information).

The UV-sensitive free radical polymerization photoinitiator is often added before the oligomerization reaction,[34,36,58,76,98,187] but this can also be done after the oligomerization is complete.[125,126,195] Photoinitiators employed here are those also commonly used for other acrylate resins, such as bis(2,4,6-trimethylbenzoyl)phenylphosphine oxide (**P1**, see Figure 5),[125,126,195] 2-benzyl-2-dimethylamino-1-(4-morpholinophenyl)-butan-1-one (**P2**),[36,76,187] 2,2-dimethoxy-2-phenylacetophenone,[34,58,98] or 2-hydroxy-4′-(2-hydroxyethoxy)-2-methylpropiophenone[189] (Table S2, Supporting Information for trade names and CAS numbers). The selection depends primarily on the desired spectral response of the initiator, for instance, when ultraviolet absorbing dyes are added to the formulation, the more specialized bis(η^5-2,4-cyclopentadien-1-yl)bis(2,6-difluoro-3-(1*H*)-pyrrol-1-yl)phenyl)titanium is advised, which is readily triggered even at $\lambda = 500$ nm (green), and thus does not suffer from light attenuation by the dye.[60]

After careful weighing of components and transferring to the reaction vessel, a solvent such as dichloromethane or tetrahydrofuran may be added to aid proper mixing,[125,126,195] but is not always required.[58,187] The amine-acrylate reaction procedure is autocatalyzed, while a catalyst is necessary for the thiol-acrylate reaction. Common, suitable catalysts are small secondary and tertiary amines, diazabicycloalkenes, or organic phosphines (Figure 13e; Table S7, Supporting Information).[194] After addition of the catalyst, the reaction initiates quickly.

The required reaction temperature depends on whether a reaction solvent is used. If so, the reaction can be performed at temperatures slightly above ambient (30 to 40 °C for thiol-acrylate,[125,126] 70 to 75 °C for amine-acrylate[36,60,76]), while if the reaction is carried out without solvent, temperatures need to be elevated to beyond the T_{NI} of the constituent reactive mesogens to aid mixing, typically 65 to 80 °C;[58,187] in the case of an amine-acrylate oligomer, even up to 110 °C.[34,58] The reaction can then be run from 30 min up to 72 h, depending on the catalyst's turnover, as well as the temperature of the reaction mixture. After completion of the reaction, the oligomer mix can be used immediately after solvent removal,[34,36,60,76,187] or can be washed using an aqueous phase to remove the catalyst.[125,126,195] The final LC oligomer ink can then be characterized with techniques such as proton nuclear magnetic resonance spectroscopy (^{1}H NMR) to gauge the average LC chain length $\overline{x}_{\text{LC}}$, gel permeation chromatography (GPC) for the chain length dispersity $Đ$, and differential scanning calorimetry (DSC) and polarized optical microscopy (POM) to investigate the mesophase transitions.

4.2.2. Adjusting Transition Temperatures

After free radical crosslinking of the just-synthesized LC oligomer mixture, a rubbery material is obtained that, if aligned, will contract significantly around the network's nematic-isotropic transition at T_{NI}. This T_{NI} is usually different from the T_{NI} of the oligomer mix before crosslinking and can be tuned by changing the monomers and molar ratios used for the LCE.

The influence of the length of the flexible alkyl spacer in the reactive mesogen seems to be a bit ambiguous; clearly, using a reactive mesogen with a C_3 spacer gives a lower T_{NI}, while

between C_6 and C_{11}, there seems to be little difference.[196] The type of mesogenic core present in the reactive mesogens also has an influence, going from a 3 to a 2-ringed core LC lowers T_{NI} of the resulting elastomer network.[197]

Amine-acrylate-based LC inks generally have higher T_{NI}s. When *n*-butylamine is used, the chain length does not appear to strongly influence the T_{NI}, varying from 94 to 115 °C.[58,191] Opting for other primary amines makes it possible to lower the T_{NI} significantly, down to 77 °C when *n*-dodecylamine is used as chain extender.[198] A wider range of possible transition temperatures has been demonstrated for LC inks based on thiol-acrylate chemistry. Using the small aliphatic ethanedithiol gave a T_{NI} of 140 °C in the final crosslinked state, whereas increasing spacer length to 11 with undecanedithiol lowered the T_{NI} to 90 °C. Using a flexible spacer based on ethylene glycol units, such as 2,2′-(ethylenedioxy)diethanethiol, has generally shown to significantly lower T_{NI} (**Figure 14** for molecular structures).[98]

Having the LCE thermal response occur at physiological temperatures, ≈37 °C, is imperative for biotechnological applications, a field where LCEs hold great promise.[199,200] The T_{NI} of an LCE can be lowered by destabilizing the mesophase of the LC. Introducing "disorder" by using multiple reactive mesogens, a flexible dithiol (1,1′-(1,2-ethanediyl) bis(3-mercaptopropanoate), Figure 14 and **Table 3**) and adding isotropic components (triallyl-1,3,5-triazine-2,4,6(1*H*,3*H*,5*H*)-trione) can lower the T_{NI} after crosslinking to 28 °C.[187] Likewise, incorporation of short poly(ethylene glycol) diacrylate (PEGDA) segments can lower the T_{NI}, although for these printability has not yet been demonstrated.[201]

4.2.3. Adjusting Mechanical Properties of the Print

Most crosslinked LCEs are soft, rubbery materials at RT, a result of their low degree of crosslinking. As a result, few differences in mechanical properties have been demonstrated between inks printed to date. For what has been reported, typical values are a storage modulus E' in the GPa range below T_g, and E' in the 10 MPa range above T_g. In general, the T_g is lower than body temperature, and for some reported printed LCE objects well below 0 °C.[126,190]

If a tougher LCE object is desired at RT, long aliphatic dithiols as chain extension agents are advised, such as 1,6-hexanedithiol, 1,9-nonanedithiol, or 1,11-undecanedithiol.[202,203] These crystallize inside the material, after which the material presents itself as a hard polymer at RT. A significant downside of this crystallization mechanism is that currently the crystallization kinetics are poor, requiring in some compositions more than 24 h for crystal domain reformation to achieve the increased toughness. When cycling temperatures quickly, these domains do not recrystallize, and the material behaves similarly to other LCE network materials.

4.2.4. Augmenting the Base LC Ink with Additional Features

Significant research on responsive LCEs that shows response to other stimulus than temperature has been reported in works not related to printing. These will be highlighted, together with selected works on LCE DIW, to serve as a source of inspiration for the design of as-of-yet nonexisting or unprinted LC inks (**Table 4**).

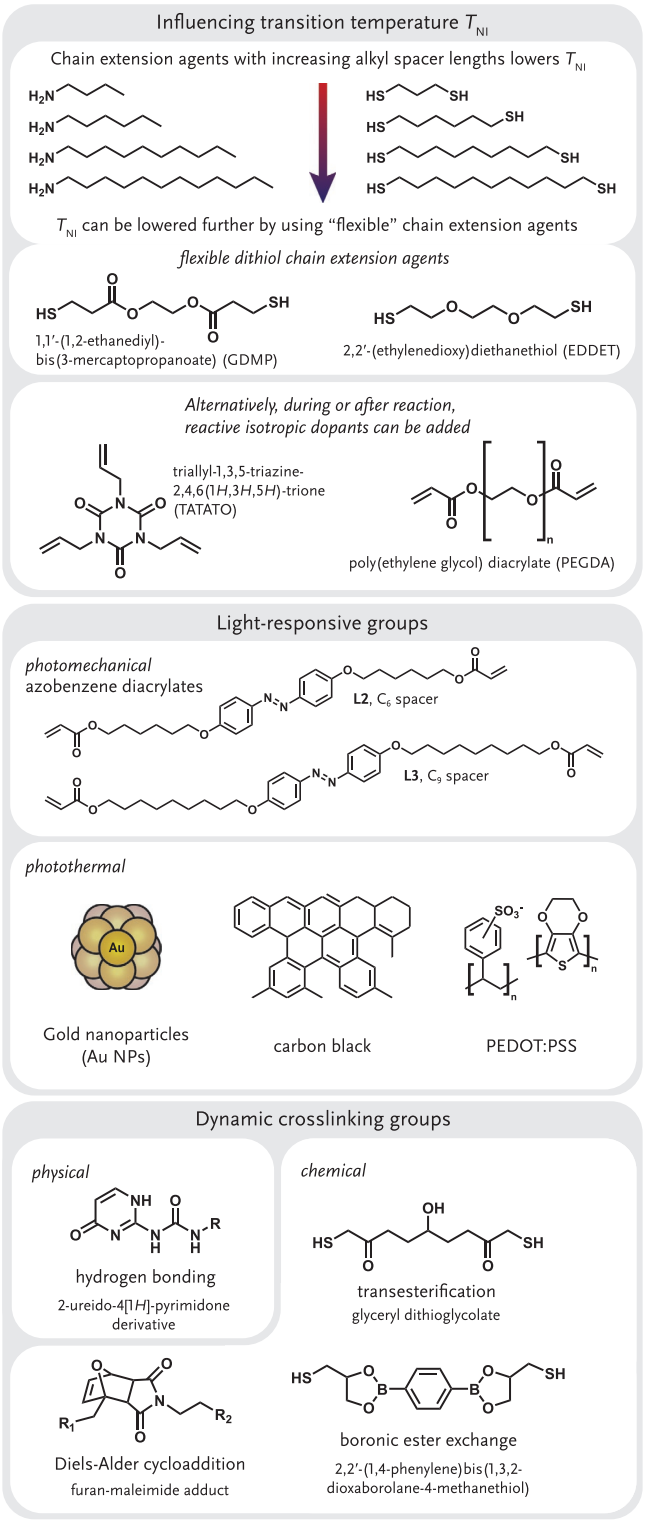

Figure 14. Dopants that have been incorporated in LCEs to achieve different functionalities, from lowering the thermal response temperature, to light response, dynamic crosslinking, and self-healing. Further information may be found in Tables S4–S6 in the Supporting Information.

Table 3. Recipes for temperature-responsive LC inks that have been printed using DIW. Molar ratios given in the same order as the components.

Desired transition temperature range	Compounds needed	Reaction procedure type	LC oligomer ink's T_{NI}	LCE's T_{NI}	Refs.
20–40 °C	Reactive mesogen: **R1**, **R2** Chain extender: 1,1′-(1,2-ethanediyl) bis(3-mercaptopropanoate) Reactive isotropic crosslinker: triallyl-1,3,5-triazine-2,4,6(1*H*,3*H*,5*H*)-trione Molar ratio: 0.43:0.37:1:0.2	Thiol-acrylate	17 °C	28 °C	[187]
	Reactive mesogen: **R1** Chain extender: 2,2′-(ethylenedioxy)diethanethiol Reactive isotropic crosslinker: triallyl-1,3,5-triazine-2,4,6(1*H*,3*H*,5*H*)-trione Molar ratio: 0.4:1:0.6		0 °C	38 °C	[187]
40–60 °C	Reactive mesogen: **R1**, **R2** Chain extender: 1,1′-(1,2-ethanediyl) bis(3-mercaptopropanoate) Reactive isotropic crosslinker: triallyl-1,3,5-triazine-2,4,6(1*H*,3*H*,5*H*)-trione Molar ratio: 0.28:0.72:1:0.2	Thiol-acrylate	29 °C	47 °C	[187]
>100 °C	Reactive mesogen: **R1** Chain extender: *n*-butylamine Molar ratio: 1.1:1	Amine-acrylate	94 °C	127 °C	[58]

Light Response: It is important to note common photoisomerizing azobenzene dimethacrylates do not participate in addition reactions forming the LC oligomers due to the significantly lower reaction rate of thiols with methacrylates compared to thiols with acrylates;[204] an azobenzene diacrylate is required if the azobenzene is to be part of the main-chain LC oligomer chain (dopants **L1** and **L2**, see Figure 14).[204] The location of the azobenzene with respect to the chain-extended LC oligomer, either in the oligomer chain, or added as a dopant after oligomer synthesis, has an effect on the actuation kinetics of photo-crosslinked LCE fibers.[125]

Other methods of creating photo-responsivity besides employing molecular photoswitches is through the incorporation of absorbing species to obtain a photothermal response instead (Section 2.2.3). This type of response to NIR light has been achieved in LCEs by adding carbon black or poly(3,4-ethylenedioxythiophene) polystyrene sulfonate (PEDOT:PSS)[199,205,206] or to visible light with Au NPs[207] (see Figure 14). Furthermore, the photothermal effect may also be initiated by dyes with narrower absorption bands, such as croconaine dyes which release heat in response to excitation at NIR wavelengths around $\lambda_{max} = 796$ nm or $\lambda_{max} = 1002$ nm, depending on the dye used.[208,209] Additionally, there are reports of LCNs that exhibit photothermal effects after incorporating a visible red-absorbing anthraquinone dye (λ_{max} = 660 nm),[210] and we expect that this dye can be easily incorporated in printable LC oligomer inks as well. An advantage of NIR conversion mechanisms (photothermal) is that high-energy UV light sources are not required. The downside is that, since the actuation mechanism is not based on a molecular photoswitch, there is no inherent mechanical "bi-stability" which might be encountered when using the photomechanical effect with azobenzene dyes with a long thermal *cis*-azobenzene lifetime.

As a result of the broad interest in phototriggered actuation schemes in LC materials, there are a number of reviews available for more, detailed information on materials choices and device architectures.[51,211]

Humidity Response: Few water-responsive LCE formulations have been reported: the apolar nature of LCs is not generally conducive for water penetrating the polymer network (Section 2.2.3). Nevertheless, two methods have shown promise for making humidity-sensitive LCEs, based on both amine-acrylate and thiol-acrylate procedures. Through the use of an *N*,*N*-dimethylaminoalkylamine as chain extension agent during synthesis, an LC oligomer is obtained with pendant tertiary amine groups.[130] After crosslinking into a network, treating with aqueous acid resulted in a hydrophilic material. Printability using DIW was shown, being similar to inks based on *n*-butylamine. Reactive poly(ethylene glycol) has been used to generate an LC block-*co*-oligomer capable of swelling in water.[129]

Electrical Response: Electrothermal heating in LCEs can be integrated by dispersing conductive eutectic metal alloys such as indium gallium (EGaIn)[132,134] throughout the LC oligomer by shear mixing. The liquid metal droplet sizes influence the bulk composite properties: at average particle diameters of ≤10 µm, actuation performance is significantly impaired compared to droplets sized 100 µm.[133]

Structural Color: The addition of a chiral dopant to the LCE formulation generates stable, structurally colored chiral nematic (cholesteric) phases that retain the characteristic chiroptical properties where only light of a single circular polarization is reflected (Section 2.2.1).[212–215] Printability of short-chain cholesteric LCEs through DIW has been reported.[64] A typical chiral dopant used for these materials at relatively low weight percentages (3.5–5 wt%) is **C1** in low molecular weight LCs.[216] In chain-extended LCEs, the weight percentage needed to maintain visible reflection increases significantly, scaling with the average chain length.[217] For an LC oligomer based on reactive mesogen **R1** and *n*-butylamine with an $\overline{x}_{LC} = 2.6$ requires 10.6 wt% of chiral dopant **C1** to reflect in the visible range.[212] It should be noted that before crosslinking of the pendant acrylate groups, the central wavelength of the reflection band strongly depends on the temperature,[212,213] leaving room for color adjustment during the final processing steps of the print.

Reconfigurability in LCE Networks: In typical crosslinked LCEs, the molecules are aligned before network formation to program the direction of actuation; the network transduces the reorientations of the mesogens into macroscopic deformation (Section 2.2.3). However, this makes LCEs somewhat limited in

Table 4. Introducing the components required for different properties of the LCE. The rightmost column indicates if these combinations have already been printed.

Functionality	Chemistry demonstrated:	Mechanism	Components used	Printed
Lowering nematic-isotropic transition temperature	Both	Lowering LC order by mixing multiple reactive mesogens	**R1** and **R2**[125,126,187]	[126,187]
	Amine-acrylate	Increasing the isotropic fraction in the LCE destabilizes the LC phase	*n*-Hexylamine[198] *n*-Decylamine[198] *n*-Dodecylamine[198] 6-Amino-1-hexanol[198]	
	Thiol-acrylate	Increasing the isotropic fraction in the LCE destabilizes the LC phase	Dithiols: 1,6-Hexanedithiol[203] 1,9-Nonanedithiol[203] 1,11-Undecanedithiol[203] 2,2′-(ethylenedioxy)diethanethiol[98,195]	
			Isotropic diacrylates: Poly(ethylene glycol) diacrylate, MW 250[201]	
			Isotropic vinyl crosslinker: triallyl-1,3,5-triazine-2,4,6(1*H*,3*H*,5*H*)-trione[187]	[58,187]
Enhancing mechanical properties	Thiol-acrylate	Include spacers that form crystalline domains	1,6-Hexanedithiol[202,203] 1,9-Nonanedithiol[203] 1,11-Undecanedithiol[203]	
Photoresponsivity	Thiol-acrylate	Photoisomerization of a crosslinked dye	(*E*)-((diazene-1,2-diylbis(4,1-phenylene))bis(oxy))bis(hexane-6,1-diyl) diacrylate[60,106,125,126]	[60,126]
			(*E*)-((diazene-1,2-diylbis(4,1-phenylene)) bis(oxy))bis(nonane-9,1-diyl) diacrylate[127]	
		Heat release by an incorporated dopant or dye	Poly(3,4-ethylenedioxythiophene)-poly(styrene sulfonate)[199,205,206]	[199,205,206]
			Poly(3,4-ethylenedioxythiophene)-poly(styrene sulfonate)[199,205,206]	
			Gold nanoparticles[207] Croconaine dyes[208,209]	
Humidity response	Thiol-acrylate	Inclusion of hydrophilic components	Poly(ethylene glycol) dithiol, MW 1500[129]	
	Amine-acrylate		2-Dimethylaminoethylamine[130]	[130]
Electric response	Amine-acrylate	Dispersion of Joule heating eutectic alloys through the LCE	Eutectic gallium indium[132–134]	[134]

Functionality	Demonstrated for chemistry:	Mechanism	Used components	Printed
Reconfigurability	Thiol-acrylate	Boronic ester exchange	2,2′-(1,4-phenylene) bis(1,3,2-dioxaborolane-4-methanethiol)[219]	
		Transesterification	Glyceryl dithioglycolate[220]	
		Disulfide metathesis	Thiol-terminated LCE oligomers and pentaerythritol tetrakis(3-mercaptopropionate), reduced with H_2O_2 and NaI to form S–S bonds[221]	
		Photoinduced reversible addition-fragmentation transfer reactions between vinyl and thioether groups	2-Methylene-1,3-propanedithiol[35,225]	[35]
	Amine-acrylate	Diels–Alder cycloaddition	Furan-maleimide adduct derivative[222]	[222]
		Hydrogen bonding	2-Ureido-4[1*H*]-pyrimidone derivative[222]	[222]
Structural color	Thiol-acrylate	Introduction of a chiral component	(3*R*,3a*R*,6*S*,6a*R*)-Hexahydrofuro[3,2-*b*]furan-3,6-diyl bis(4-((4-(((4-(acryloyloxy)butoxy)carbonyl)oxy)benzoyl)oxy)benzoate)[64,212–215,217]	[64]

their use, in the sense that whatever alignment is programmed into this network will permanently dictate the macroscopic deformation of the device.

In recent years, concepts from research on dynamic covalent chemistry (DCC) and vitrimers have made their way to LCEs to allow for self-healing devices, or recycling of actuators and

reconfiguration into alternative actuation pathways to those initially generated.[218] The dynamic chemistries can be roughly divided into thermally initiated and photoinitiated moieties.

Thermally initiated mechanisms include boronic ester exchange reactions,[219] transesterification,[220] disulfide exchange reactions,[221] and Diels–Alder cycloadditions coupled with hydrogen bonding.[222] LCE networks containing boronic ester and free hydroxyl groups have been reprogrammed by heating to 80 °C while straining the network;[219] cleavage of disulfide groups requires significantly more energy, with heating to 180 °C required to cleave all S—S bonds.[221] Combining orthogonal supramolecular bonding schemes in one device is also possible, as shown by utilizing furan, maleimide and ureidopyrimidone groups in a single amine-acrylate LCE.[222] Furan and maleimide form a Diels–Alder cycloaddition adduct and a dynamic covalent bond,[223] thermally reversible at ≈110 °C in this LCE system. 2-ureido-4[1*H*]-pyrimidone (UPy) groups form self-complementary quadruple hydrogen bonded physical crosslinks,[224] which in the LCE system here cleave at around 50 °C. Combining two dynamic crosslinking groups without any permanent covalent crosslinks leads to a material that can be reconfigured at relatively low temperatures, and recycled at elevated temperatures.

An important consideration in designing LC oligomer inks containing supramolecular crosslinks is the presence of two concurrent, thermally activated processes: dynamic bond reorganization and isotropization of the LC. For actuator devices that rely on the nematic–isotropic transition, this introduces the risk that in the actuated state, the LCE device also changes its network topology to relax stress, and refixes itself in the isotropic state. This can be avoided by choosing dynamic covalent groups with sufficiently high reconfiguration temperatures, such as the furan–maleimide combination,[222] with LC inks that actuate at low temperatures, such as those with a high fraction of isotropic component.[187,201] Alternatively, the LCE actuation and bond reconfiguration can be decoupled by making one of the two photoactivated by incorporating free vinyl groups in the LCE through the use of a molecule such as 2-methylene-1,3-propanedithiol.[35,225] Since this reconfiguration mechanism requires available photoinitiator, these formulations generally contain two photoinitiators which are triggered at different wavelengths, the first one used to crosslink the LC oligomers immediately after printing, the second for reconfiguration.

4.3. 4D Printed Centimeter Scale LC Structures

4.3.1. Soft Robots

In most work detailing printed LCEs, uniaxially aligned strips are a common design since these allow intuitive gauging of the LCE's thermomechanical properties.[34,36,60,76,188] Load-free thermal contraction is generally in the order of 40%–50%,[34–36,58,76,98,187,226,227] with actuation stresses in the kPa range at low strains.[98,227] The contracting strips may be used as "artificial muscle" in its simplest setup: lifting a mass vertically against gravity (**Figure 15**a).[36,76] Both single fibers extruded

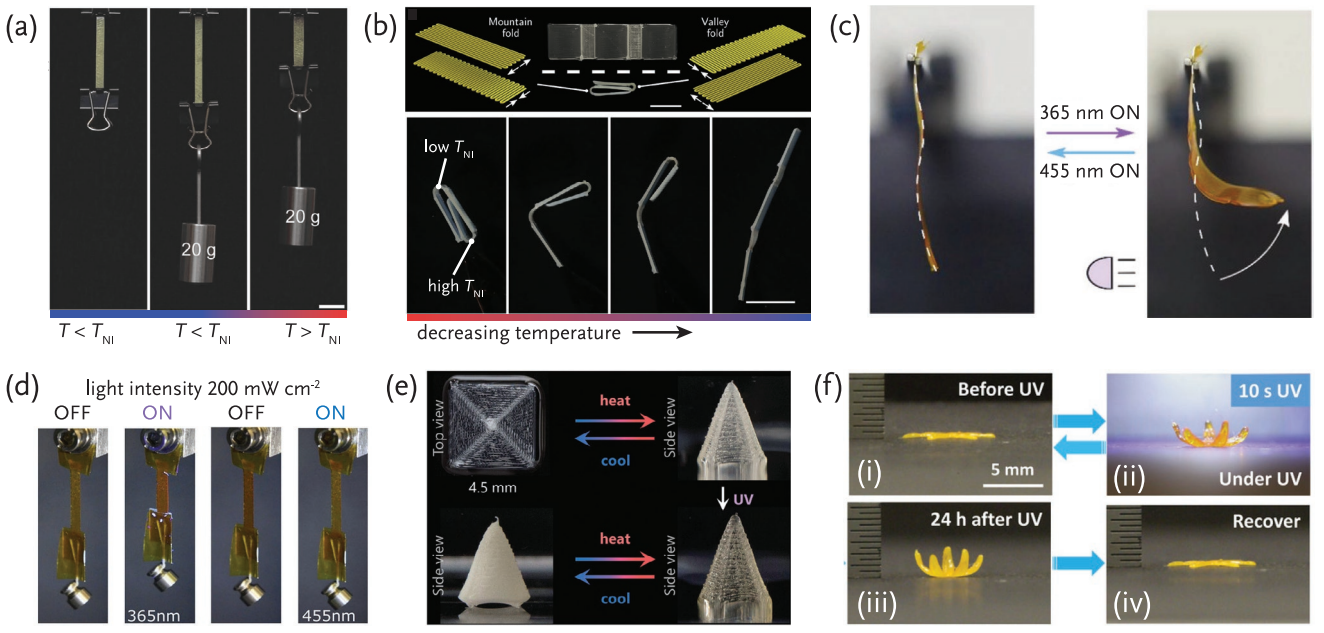

Figure 15. a) Soft actuator showing "artificial muscle" function. Adapted with permission.[34] Copyright 2018, Wiley-VCH. b) Using bilayers with perpendicular alignment over the two layers, controlled bending can be induced, and by combining LCEs with different T_{NI}, step-wise actuation schemes can be created. Adapted with permission.[58] Copyright 2019, American Association for the Advancement of Science. c) Azobenzene-containing printed LCE showing light-induced bending, in this case away from the light source. Reproduced under the terms of the Creative Commons CC BY license.[126] Copyright 2020, Wiley-VCH. d) Light-addressable "artificial muscle." The material is similar to that shown in panel (c), but adding a bias load leads to linear contraction rather than bending. Reproduced with permission.[60] Copyright 2020, American Chemical Society. e) Print containing a +1 point defect that pops out into a cone upon heating, and can be permanently fixed in this shape using pendant photoreactive groups. Reproduced with permission.[35] Copyright 2019, Wiley-VCH. f) Device i) that responds by bending after addressing the incorporated azobenzene molecules ii), while the heat generated in this process releases hydrogen bonds that reform after illumination is ceased iii). By heating and breaking these bonds without UV, the object returns to the original shape iv). Adapted with permission.[222] Copyright 2020, Wiley-VCH.

using direct ink writing and multiple printed fibers woven into conventional textiles have been used to embed smart properties in otherwise static materials.[227]

The ability to lift weights is often quantified using the mass-based work capacity[203,228]

$$\frac{W}{m} = \frac{\sigma_{bias}\varepsilon_a}{\rho}\left[\mathrm{J\ kg^{-1}}\right] \quad (7)$$

Work capacity values are often not clearly reported in the literature: some report this value using $L_0 = L$ at RT in the loaded state,[203] while others use the load-free state.[34] Typical reported values for the volumetric work capacity are on the order of 1–40 J kg^{-1}, which puts it in the same order of magnitude as mammalian skeletal muscle (≈8 J kg^{-1}).[229] Compared to LCE films made in the conventional two-step process, work output in printed devices is a little lower, likely a result of the reduced molecular order.[229,230]

Incorporation of an azobenzene photoswitch in the oligomer chain makes the contraction light-addressable (Section 2.2.3). In load-free nematic azobenzene-LCEs, the light-triggered contraction along the alignment direction of the LCE leads to a bending motion toward the light source; as the excitation light for the azobenzene is gradually attenuated, a concentration difference in the *cis* and *trans* isomers forms through the depth of the film, and thus a gradient in contraction (Figure 15c). Loading the sample with a mass results in a linear contraction after illumination with λ = 365 nm light,[60] the contractile strain proportional to the light power, with a maximum of 32% (Figure 15d). During this maximum contraction, 12 J kg^{-1} of specific work was generated.[229] Light-responsive actuators with tunable bending directions were printed using a modified LC ink in the smectic C mesophase as well.[126] This latter work also demonstrates that both elongation and contraction can be performed underwater.

Through engineering the molecular director, a variety of macroscopic deformations can be created: by printing two layers of LCE in orthogonal printing directions, thermo-responsive hinges are formed (Figure 15b).[58,188] Upon heating, these hinges can generate appreciable amounts of torque (1 mN m), comparing favorably to torques exhibited by hinges based on shape memory polymers.[58,188,231] A porous woodpile structure contracts in both length and width with increasing temperature, while the printed structural "beams" increase in diameter, lowering overall porosity. Heating or cooling a "+1 point defect" spiral shape causes directional expansion or contraction along the mesogenic alignment direction, resulting in an out-of-plane deformation forming cone-like or saddle shapes that can be used to lift weights from below (see Figure 6c). Bistable architectures can be generated by printing a spiral structure with inner and outer parts having opposite Gaussian curvatures, so heating builds stresses between these two parts that are released as a "snapping" motion, capable of lifting 5× the mass of the actuator.[76] Combining multiple inks of different T_{NI} in a single cone leads to two-stage actuation.[187]

A fixable 2D-to-3D cone-forming actuator was shown based on a reconfigurable LC ink. After printing into a spiral pattern and crosslinking, the sheet forms a cone-shaped protrusion as the surrounding temperature is increased.[35] Illuminating the object with UV light activates the remaining photoinitiator, triggering free vinyl groups to cause a network rearrangement. After this reaction, while the LCE can internally still change between polydomain nematic and isotropic phases, the new, conical shape of the device is fixed (see Figure 15e). Using physically crosslinking UPy groups, the actuated state after UV illumination can be fixed in temporarily and reversibly (see Figure 15f).

The freedom provided by direct ink writing allows for the fabrication of responsive objects guided by mechanical metamaterial principles, such as auxetics.[98] In such designs, the contraction caused by a small amount of LCE is transduced into a much larger dimensional change in the printed object.

4.3.2. Biomedical Implants

While LCEs have not yet been approved for use in human implants, research has suggested a degree of biocompatibility,[192] opening a whole vista of possibilities (**Figure 16**). Based on the thermal contraction programmable through direct ink writing, urological implant concepts were demonstrated[199,205,206] based on an LCE with low T_{NI},[187] which were doped with carbon black to induce photothermal heating via infrared light which passes through biological tissue relatively well (Figure 16e).[199,205,206,232]

Medical applications of LCEs do not always rely only on thermal contraction: DIW was used to print a prototype intervertebral implant which uses a crystallizing resin formulation. During implantation, the soft LCE conforms to its environment, after which it slowly crystallizes (Figure 16a,b). This prototype shows excellent fatigue properties, barely showing any permanent deformation over one million compression cycles, opening up the option to print personalized implants in future.[62] The high T_g (>RT) of the crystalline LCEs allows for programming an additional one-way shape memory effect to complement the two-way shape change inherent to the LCE's nematic–isotropic transition. This effect was harnessed to design a cardiovascular stent that can be folded for insertion in the body, where it can subsequently assume its active shape, able to expand and contract around T_{NI}.[203]

Significant for in vivo applications is the observation that reactive oxygen species, such as aqueous H_2O_2, oxidize the thioether linkages in thiol-acrylate LCEs, transforming the ordinarily hydrophobic LCE into a hydrophilic material that swells in water (Figure 16c,d). Since this swelling is directional, the initial print path used during device printing steers the final shape after water absorption.[61] This design possibility can be used to generate implants that fold or bend into shape after insertion in a biological environment.

4.3.3. Photonic Devices

Contrasting the widespread use of LCs in optical engineering, centimeter scale printing of LC optics has only rarely been demonstrated. For example, an adjustable lens was made

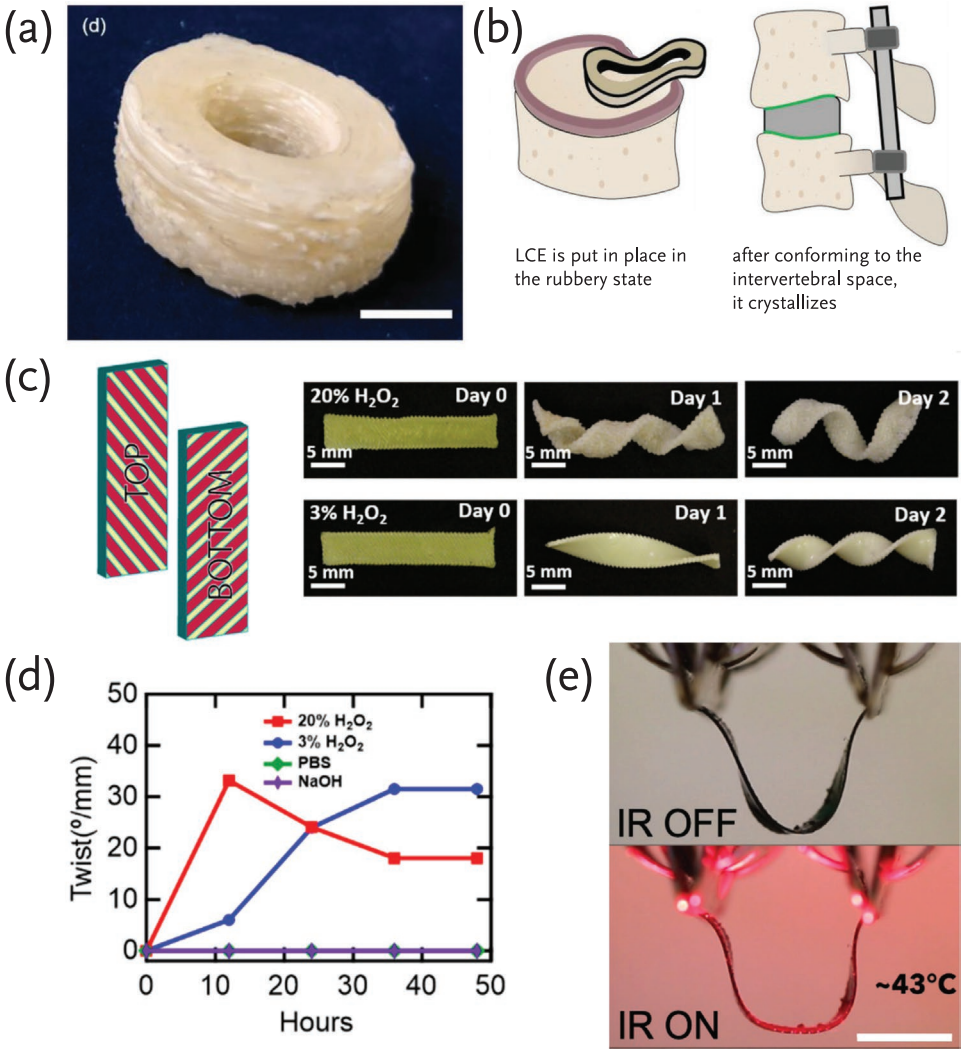

Figure 16. a) Direct ink written intervertebral implant based on a thiol-acrylate LCE. b) The implant from panel (a) is put in place in the rubbery state and conforms to the intervertebral space in this state. Over time, the material, based on a long aliphatic dithiol (*n*-decanedithiol), crystallizes and hardens, from there on supporting the vertebrae. c) A strip of LCE that becomes hydrophilic in oxidizing media and responds by swelling directionally. In this case twisting, as expected from the displayed mesogen alignment. d) Degree of twist for the LCE film in panel (c) for a variety of chemical environments. e) Implant concept that deforms when heated photothermally using infrared light. a,b) Adapted with permission.[62] Copyright 2019, Wiley-VCH. c,d) Adapted under the terms of the Creative Commons CC BY license.[61] Copyright 2020, MDPI. e) Reproduced with permission.[199] Copyright 2020, AIP Publishing.

by combining a printed ring of thermally responsive LCE in a static, compliant PDMS slab.[36] By designing the infill to follow a concentric pattern, heating the composite causes in-plane ring shrinkage, pushing out the clear PDMS, resulting in temperature-sensitive light refraction (**Figure 17**a). In another example, a responsive linear polarization filter was demonstrated by printing a chiral holder, in which the center element rotates as the outward spanning fibers contract.[36] This contraction rotates a small linear polarizer placed in the holder, which, when coupled with a second, static polarization filter, forms a thermally addressable, variable transmission element (Figure 17b).

Direct printing of a structurally colored material was achieved using a chiral nematic LC ink from the isotropic phase onto a heated print bed at low printing speeds (≈1–2 mm s^{-1}, Figure 17d),[64] making it possible to print objects with optical behavior similar to chiral nematic films fabricated in specialized LC alignment devices.[53] By printing at greater speeds (≈8–10 mm s^{-1}), the normal helical alignment of the chiral nematic was distorted, forming anisotropic reflectors (Figure 17c). Combining varying print paths and speeds, it is possible to write optical elements with highly perspective-dependent appearances.[64] Consequently, the reflected polarization state can be controlled through the print parameters, as the distorted helical alignment does not discriminate between left- and right-circular polarized light at normal incidence, unlike conventional chiral nematic reflectors or those printed at lower speeds which are exclusively selective to either right- or left-circular polarizations at normal incidence.

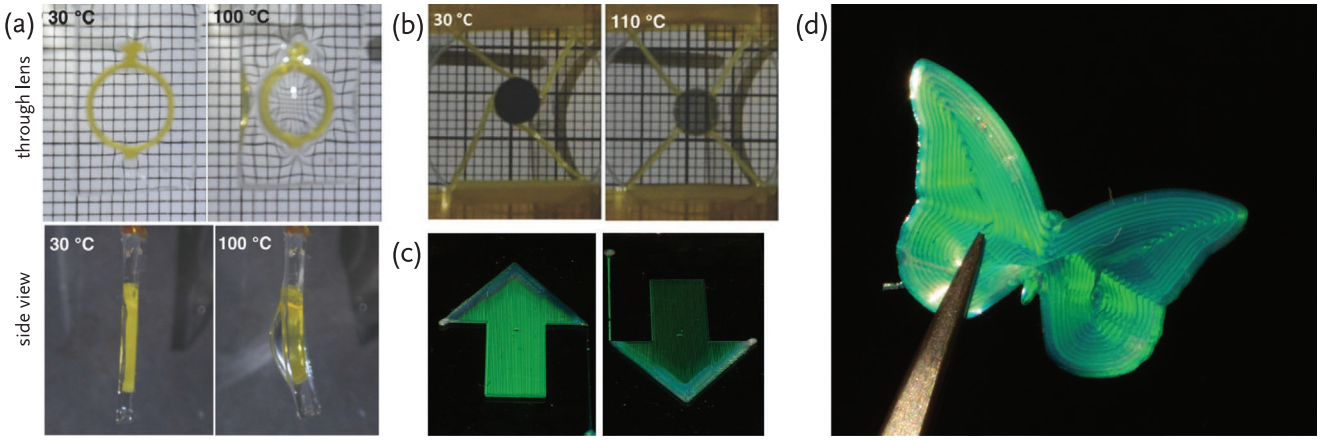

Figure 17. a) LCE-PDMS composite structure. The LCE is printed in a ring that effectively is a section of a +1 point defect. With increased temperature, the ring diameter diminishes, pushing out PDMS bound to it. This is seen in the side view. The transparent PDMS acts as optical element of varying focal point distance depending on its curvature. b) Chiral architecture in which a small linear polarization filter is rotated to reveal the image behind it. c) Reflective optical element, the appearance of which was encoded by direct ink writing at high nozzle speed. Depending on the perspective of the viewer with respect to the object, it is either bright green, or very weakly colored. d) Free-form reflective optical element that was direct ink written at low nozzle speed. After release from the substrate, a self-supporting photonic object is obtained. a) Adapted and b) Reproduced with permission.[36] Copyright 2017, Wiley-VCH. c,d) Reproduced under the terms of the Creative Commons CC BY license.[64] Copyright 2021, Wiley-VCH.

5. The Future of Liquid Crystals in 4D Additive Manufacturing

As can be gauged from the concepts and examples presented in this Review, many different research avenues have already been explored. However, there is still considerable room for future developments, both in terms of the feedstock materials as well as AM processes. The field of 4D printing with LCs is still in its infancy, which means that considerable knowledge acquired from previous studies of LCN films, actuators, and LCD screens has not yet been exploited by AM techniques. Reactive LCs might not achieve the commodity status of common polymers; most AM techniques are not suited for mass production, yet we feel 4D printing can help meet future needs for biomedical applications or personalized soft human-interface devices, for instance. This Section presents possible future research avenues according to these future needs, and what logically follows from the current literature landscape.

5.1. New Materials and Properties

Unexplored Stimuli: While we cannot envision using magnetism as a method to address specific regions of devices constructed from LCs, it could find use as larger-scale force field to move a bulk device,[136] such as through bodies of water or biological tissues. Sensitivity to specific chemical analytes could be interesting as triggers for autonomous guidance of soft robots: solvent responses have already been shown for LCEs.[115,217] As an example of responsivity to specific chemicals, cholesteric LCNs responsive to volatile amines released from decaying biological matter showed a visible color change.[117] Developing chemical-sensitive LCEs could be the first step toward soft robots that autonomously navigate chemical gradients, or, when developed as cholesteric LCEs, act as printable optical chemical sensors for use on the outside of the body.

Complementary Stimuli LCs and Multifunctional Devices: There already is widespread knowledge on the combination of functionalities and/or responses in a single LCN formulation to obtain humidity- and chemical-sensitive optics,[117,233,234] humidity-gated UV-responsive actuators,[110] or humidity-gated temperature-responsive IR reflective coatings.[235] These systems benefit from additional properties, or increase control of the device performance thanks to these double functionalities or responses. Translating these combinations into extrudable LCEs, which as shown in Section 4 are highly modular, or into LC photoresists for TPP-DLW as recently suggested with the fabrication of photonic microactuators,[59,181] would be of great interest. An elegant example of the possibilities offered by this modularity is a structurally colored LCE which combines shape reconfigurability with the optical properties of a cholesteric.[236] Unfortunately, these combinations have not been yet investigated in LCEs suitable for 3D microextrusion, and remain an exciting avenue to explore.

Different Reactive Mesogen Chemistries: So far, most RM formulations for AM that have been reported make use of acrylate free-radical polymerization for final crosslinking steps. Significant downsides of radical polymerization reactions is that these are notoriously sensitive to chain growth termination by atmospheric oxygen, and suffer from polymerization shrinkage.[161] Epoxide and oxetane moieties as reactive groups, both of which polymerize through a cationic mechanism, have been limitedly explored in thin-film LCNs and the former also in TPP-DLW.[158] For DIW with LC oligomer inks, these have not been reported yet. While results described for acrylate-based inks in DIW have not uncovered large issues, having oxygen-insensitive inks could help in ensuring the highest possible polymerization conversion and thereby long-term object integrity.

Self-Healing Materials and Environmental Considerations: Something that has also gone underexplored on the chemical side of LCE research is the development of recyclable LCE materials. Recyclability becomes increasingly important as the volumes of LC materials increase to meet the demands of producing soft robots and large-scale actuating objects. Given that most polymeric LC devices currently are thermosets which are difficult to recycle, most will end up in landfills after use, or are mechanically ground down into low-quality filler materials.[237] The development of more sustainable LC materials for additive manufacturing can be approached by: 1) development of self-healing dynamic covalent crosslinked LC formulations, 2) thermoplastic LC design, or 3) LC mesogens that can be degraded in a functional manner. A final option, 4) design of liquid crystalline materials based on renewable sources, should also be investigated.

One of the foremost solutions (option 1) is to develop thermosets with reversible crosslinks, which would allow for reconfiguration of the material into new shapes, or complete melting for recycling. At the same time, many chemistries that allow for reconfigurability also inherently bring (self-)healing capabilities, which would extend the useful lifetime of the materials. Chemistries that can be employed for this purpose have been briefly highlighted in Section 4.2.4; namely dynamic covalent or physically crosslinking groups.

Currently, thermoplastic LCs (option 2) are mainly limited to engineering polymers such as Kevlar or Vectra, which show extraordinary Young's moduli but also require harsh conditions for processing: Kevlar is spun from concentrated H_2SO_4[238] and FFF of Vectra requires nozzle temperatures above 280 °C.[69] Furthermore, while they share the strong anisotropy found in LC materials, importing the functionalities known from LCNs and LCEs into the polymers has not yet found widespread attention. Developing thermoplastic LCEs could be the middle road here, where short chains of LC oligomers physically bind. Since the material originates as a reactive mesogenic oligomer, this leads to easy incorporation of functional groups known from LCN and LCE research into the chains, while the physical crosslinking allows for remolding, reshaping, and eventually, recycling.

Easy breakdown of crosslinked LC materials (option 3) would require the design of new mesogens with labile chemical groups. Nonmesogenic formulations have been developed for TPP-DLW that makes use of silyl ether groups which readily disintegrate in alkaline conditions, depending on the substituents on the labile group.[239]

Securing a sustainable future for the materials presented in this review also requires reviewing methods of synthesizing mesogens from renewable sources instead of from the petrochemicals that many organic compounds are currently derived from (option 4). Such a route is to consider alternative natural materials that show LC properties. An example of this are aqueous dispersions of cellulose nanocrystals which display cholesteric phases at specific concentrations.[240,241]

Optical Performance of Printed Structures: As exemplified in many reports of LCEs printed using DIW, it is clear that the imperfect mesogen alignment brings about a milky, scattering appearance.[36,76,187,227] When the printed LCE is to be used in optical processes, such as light-triggered actuation[60,126] or as reflective elements,[64] light scattering can be detrimental to the LCE's function, preventing precise focusing of light for actuation, or a reduced quality reflector. This is exacerbated if thicker layers are printed, or multiple layers are printed on top of each other. Ideally, it should be possible to print LCEs with a homogeneous, optically clear appearance, mostly through tuning the deposition procedure. Another option to improve transparency could be to include a surfactant in the printing ink to assist LC assembly at the LC–air interfaces.

5.2. Additive Manufacturing Processes

To date, a few AM techniques have been shown applicable for LC-based materials. While DIW and TPP-DLW have led to promising results and interesting devices, we feel that there are plenty of remaining techniques that can fill specific niches when combined with an LC feedstock. Some of these processes have been demonstrated just once, while others have not been reported at all. We provide some of our own visions.

Vat Polymerization: A key challenge for any vat polymerization is the relative volume of material required in the vat itself. Generally, LC-based materials are not inexpensive, and there is considerable "wasted" volume that makes most conventional vat polymerization setups, e.g., SLA or DLP, cost-prohibited. Of course, this may be alleviated by restructuring the vats to accommodate smaller volumes. A second challenge is achieving alignment. Since alignment is key to harnessing the unique properties of LC materials, it is not a trivial task to print LCs layer-by-layer and maintain proper alignment characteristics. Presumably, a thin enough alignment layer applied to the baseplate would allow alignment of the initial layers, but subsequent layers would need to rely on the already-deposited layers, so rapid degradation of the alignment fidelity would be expected.

TPP-DLW: When considering the use of LC photoresist in a TPP-DLW, there is one big limitation that comes from the equipment: commercial printers do not have a heating stage incorporated. As a result, the possibility to use well-known and quantified LC mixtures directly in TPP-DLW set-ups is not possible since RM mixtures with room temperature liquid crystalline phases are uncommon and challenging to prepare. These challenges unnecessarily slow down progress on LC-based microdevices. Additionally, it has been shown that control over the temperature during the TPP-DLW process can reduce the swelling of the polymerized structure during fabrication and so enhance resolution of the LC microstructures;[157] thus, investing in a custom-made heating stage might be of significant value.[157,158]

While TPP-DLW can print with outstanding resolution, it comes at a high price: its production speed for large quantities of microstructures is extremely low. While for fundamental research application this is not a problem, it limits its possibilities to compete with other AM techniques in industry. In order to solve this, efforts are being made to increase the production speed by focusing multiple laser beams in the vat at the same time, by developing stages with faster scanning speeds, and by exploring quicker polymerization mechanisms.[242,243] While these advances are still at its infancy, they show promising results toward faster production speeds for TPP-DLW.

As mentioned in the previous section, multifunctional objects are of increasing interest for many reasons. We already discussed in Section 3 some examples in which multiple materials were combined in a single structure using TPP-DLW.[30,31,162] However, various steps were necessary which made the fabrication process tedious and long. Recently, TPP-DLW inside a microfluidic device was presented as a facile approach to accomplish multimaterial microobjects.[244] We believe that these kind of innovations when translated for LC photoresist, will step up the design and complexity of responsive microstructures.

DLP: As discussed in Section 3, light-based manufacturing techniques such as TPP-DLW are often combined with alignment layers or cells to ensure proper orientation of the molecules for the intended function after the AM procedure. At the millimeter scale, a similar technique is digital light processing, although the issue here is the moving printer parts between light exposure steps may disturb the molecular alignment and make it difficult to easily fit alignment layers around the LC resin. Nonetheless, 3D LCN object have been made through a magnetic field-aligned DLP procedure.[37] This alignment procedure could be extended to LC elastomer materials by using magnetic fields (**B** = 300 mT) to (re)align the LC monomers before crosslinking.[245] The LC elastomer used in the latter work is a "side-on" LC, a reactive mesogen with acrylate moiety fixed to the central phenyl ring of the mesogenic core. After crosslinking such LCs, more freedom in movement is retained, leading to larger actuator responses. Both works also incorporated diacrylate azobenzene photoswitches and demonstrated photoinduced bending in their engineered structures. While one of the advantages of DLP is that it can utilize low molecular weight LCs, which is generally not possible in DIW for production at the centimeter scale, LC elastomers should be more appropriate in large range-of-motion actuator designs.

3D Microextrusion: It is generally greatly desirable for fully printed functional devices to be made of more than a single material.[58] Using nonresponsive, mechanically superior materials as the skeleton of a device allows for application of the generally more expensive, responsive elements just as the actuating hinges, rather than designing the entirety of the object to out of LCs. A way of combining different material properties is through coaxial DIW, where filaments are formed consisting of a heterogeneous core–shell makeup. In such architectures, the inner and outer regions can perform different functions, such as a core that contracts upon heating with an outer layer that is optically active, or a core that conducts electricity or heat and an actuating outer shell that bends or twists.

A completely different way to use DIW compared to as discussed in Section 4 harkens back to the original processing of LCEs: crosslinking after mechanical stretching of a partially polymerized network.[192,193] This stepwise fabrication of a monodomain, uniaxially aligned LCE was also used for thiol-acrylate-based LCE slabs.[192] Since after the first partial polymerization step a network is created that cannot be extruded, a workaround is needed for adaptation to DIW. The solution is dividing the first step into two:[189] synthesizing a partially crosslinked LCE network with only a fraction of the final amount of thiol groups and adding to the printing syringe, along with the amounts of unreacted di- and tetrathiol required for proper conversion of the acrylate groups. After DIW printing into a solvent bath containing thiol-acrylate catalyst, the partially crosslinked printed network swiftly incorporates the thiol monomers to fully crosslink. This 3D written material can then be dried, deformed, and photopolymerized with UV light. During deformation, the LCE mesogen alignment reorients such that when thermally activated, the printed object shifts between the "as-printed" and "as-deformed" states. While printing into the solvent bath significantly reduces printing resolution, physically shaping the low-temperature actuation state through physical molding circumvents the need for the (sometimes impossible) design of intricate molecular director patterns and suitable print paths.[189]

LCs have found limited use with FFF, which mainly comes down to material properties. Typical stimuli-responsive LCs are a viscous liquid or resin before crosslinking, meaning that fabricating a solid-state filament spool is not possible. Obviously, processing crosslinked LCNs is not possible with FFF either, although the development of LCEs with reversible, physical crosslinks might prove an entry point of stimulus-responsive LC materials to FFF. So far, the only currently reported LC materials that have been processed using FFF are high molecular weight thermoplastic LC polymers, such as the engineering plastic Vectra.[69] Here, the strongly anisotropic properties of this material were encoded in computer-designed objects designed to have high-impact resistance, or act as load-bearing biomedical implants.

A slightly different approach toward incorporating densely crosslinked LCNs in an FFF procedure was demonstrated by using stimuli-responsive LC network flakes as dopant in conventional 3D printing polymer filament.[246] However, in this first report the flake response was not maintained after printing as a result of the humidity response of the LCN flake dopant being compromised by the barrier properties of the host polymer. Finding or developing more suitable water-permeable host polymers, or a new LCN formulation that works in this confined environment would open up a myriad of possibilities, given the widespread use of FFF printers and the current boom in filament material development.[1,247,248]

Other Techniques: Among drop-on-demand manufacturing techniques, inkjet printing (IJP) is the most common, and has been used for additive manufacturing of a variety of devices, organic LEDs, organic photovoltaics, and hydrogels.[249,250] When used with crosslinkable inks, this technique can be used to build multimaterial polymer objects at high resolution.[251] For LCNs, this technique has been demonstrated, where through a combination of different LC formulations and sacrificial layers, a "cilia array" was printed, built up by segmented films emulating the motion cycle of cilia in the human lungs.[252] Despite this promising result, we are not aware of any follow-up efforts using inkjet printing to produce LC-based devices.

An avenue that has not been explored at all but we deem to be promising is to use LCEs in inkjet printing, as these show larger actuation strokes: however, the increased viscosity of these materials may prove a significant obstacle to overcome for IJP. In addition, any alignment of the LC will need to rely on substrates, which will also limit the structures achievable.

Combining Multiple AM Techniques in the Same Printer: As shown throughout this Review, LCNs and LCEs provide significantly different responses to stimuli, so combination of these two materials, which also have distinct mechanical properties, in a single object through the use of AM techniques best suited for each material could open new avenues for the design of 4D objects and their achievable responses. For that, the design of multiprocess printer that combines multiple AM technique in one set-up are of interest. Intriguing developments in this direction are the recently reported set-ups that combine inkjet printing and direct ink writing[253] or digital light projection with DIW.[254] These two examples show how it could be possible to combine in a single object the different mechanical properties and types of response of LCNs and LCEs, an exciting new line of research.

5.3. Considerations on Device Design

The combination of additive manufacturing techniques with liquid crystals can lead to functional objects that self-propel,[58] walk,[159] grasp,[30] and act as optical sensors.[59] When designing LC-based 4D objects, not only does the geometry need to be carefully chosen to perform the desired tasks, but the mesogenic alignment must also be precisely selected. As discussed in Section 2.2.3, changes to geometry and/or alignment can both lead to significantly different deformation modes. For instance, identical shapes with differing alignments[33] or the same alignments in different geometries[108] can result in distinctive actuations. In Sections 3 and 4, we presented examples of this tunability of the performance of LC-based object; however, most deformation modes reported to date can be predicted using digital modelling.[102,103,131,255,256] Through simulation the interaction of alignment and geometry can be exploited to determine the optimal configuration for the desired device. For example, origami- and kirigami-inspired actuators[257] will considerably benefit from using such models. By using simulations to design LC-based objects via AM, new vistas of responsive devices that could be imagined but were not possible to fabricate just a few years ago could be revealed.[258]

6. Conclusions

Mostly due to economics of scale, additive manufacturing is positioning itself as a small-scale manufacturing technique for prototyping or producing short production runs of one-offs.[259] For most materials, conventional techniques such as casting, molding, or extrusion are more cost-effective at large production runs. However, in the case of reactive LC materials where molecular alignment is key, DIW is positioning as the best technique for the fabrication of centimeter scale objects and might well develop into a manufacturing technique at all production scales. Compared to conventional techniques, DIW allows for easy programming of the molecular director and thus anisotropic mechanical properties. Similarly, vat polymerization techniques such as two-photon polymerization-direct laser writing and digital light projection are unlikely to conquer the mass market when used for reactive LC materials, but can fill very specific niche uses. In the case of TPP-DLW, highly accurate reproductions of CAD designs at the micrometer scale can be designed, possibly for use in biomedical engineering. DLP, combined with a suitable alignment technique, can be used to make solid LC devices at the centimeter scale in all dimensions, x, y, and z.

We have demonstrated the potential advantages of printing anisotropic, reactive LC-based materials, and how they can provide responsive materials with unprecedented control over actuator motions and visual changes. It is our hope that this Review has inspired the reader to either take up 3D printing of their LC-based materials or has provided a guide on how to get started using LC materials in your AM machine of choice. The goal is now to find appropriate materials and techniques for applying these materials to achieve these lofty application goals, and this can only be accomplished by bringing in more researchers with fresh perspectives to the field, combining knowledge from materials and printing experts to meet these challenges.

Supporting Information

Supporting Information is available from the Wiley Online Library or from the author.

Acknowledgements

M.d.P. and J.A.H.P.S. contributed equally to this work. The project partners in the DynAM project consortium ("Dynamic Materials for Additive Manufacturing"), specifically, Dr. Tessa ten Cate (TNO), are thanked for critical discussions and technical insights. The colleagues who were haphazardly asked to judge figures-in-development are also thanked for their opinions and critiques. The authors' research was funded by the Dutch Research Council (NWO) in the framework of the Innovation Fund Chemistry and the Dutch Ministry of Economic Affairs and Climate Policy in the framework of the PPP allowance.

Conflict of Interest

The authors declare no conflict of interest.

Keywords

4D printing, additive manufacturing, direct ink writing, liquid crystals, stimuli-responsive materials, two-photon polymerization direct laser writing, two-way shape memory

Received: June 8, 2021
Revised: July 20, 2021
Published online:

[1] S. C. Ligon, R. Liska, J. Stampfl, M. Gurr, R. Mülhaupt, *Chem. Rev.* **2017**, *117*, 10212.
[2] F. Bos, R. Wolfs, Z. Ahmed, T. Salet, *Virtual Phys. Prototyp.* **2016**, *11*, 209.
[3] A. J. Gross, K. Bertoldi, *Small* **2019**, *15*, 1902370.

[4] H. Klippstein, A. Diaz De Cerio Sanchez, H. Hassanin, Y. Zweiri, L. Seneviratne, *Adv. Eng. Mater.* **2018**, *20*, 1700552.
[5] (Eds: F. Froes, R. Boyer), *Additive Manufacturing for the Aerospace Industry*, Elsevier, Amsterdam **2019**.
[6] D. J. Wu, C. V. C. Bouten, P. Y. W. Dankers, *Curr. Opin. Biomed. Eng.* **2017**, *2*, 43.
[7] S. Ostrovidov, S. Salehi, M. Costantini, K. Suthiwanich, M. Ebrahimi, R. B. Sadeghian, T. Fujie, X. Shi, S. Cannata, C. Gargioli, A. Tamayol, M. R. Dokmeci, G. Orive, W. Swieszkowski, A. Khademhosseini, *Small* **2019**, *15*, 1805530.
[8] S. V. Murphy, A. Atala, *Nat. Biotechnol.* **2014**, *32*, 773.
[9] R. Karyappa, M. Hashimoto, *Sci. Rep.* **2019**, *9*, 14178.
[10] J. I. Lipton, M. Cutler, F. Nigl, D. Cohen, H. Lipson, *Trends Food Sci. Technol.* **2015**, *43*, 114.
[11] M. Moini, J. Olek, J. P. Youngblood, B. Magee, P. D. Zavattieri, *Adv. Mater.* **2018**, *30*, 1802123.
[12] A. Paolini, S. Kollmannsberger, E. Rank, *Addit. Manuf.* **2019**, *30*, 100894.
[13] J. S. Lee, *J. Fash. Bus.* **2020**, *24*, 130.
[14] M. R. Hartings, Z. Ahmed, *Nat. Rev. Chem.* **2019**, *3*, 305.
[15] F. Kotz, P. Risch, D. Helmer, B. E. Rapp, *Adv. Mater.* **2019**, *31*, 1805982.
[16] M. R. Chowdhury, J. Steffes, B. D. Huey, J. R. McCutcheon, *Science* **2018**, *361*, 682.
[17] S. H. Park, R. Su, J. Jeong, S.-Z. Guo, K. Qiu, D. Joung, F. Meng, M. C. McAlpine, *Adv. Mater.* **2018**, *30*, 1803980.
[18] S.-Z. Guo, K. Qiu, F. Meng, S. H. Park, M. C. McAlpine, *Adv. Mater.* **2017**, *29*, 1701218.
[19] X.-Q. Wang, K. H. Chan, Y. Cheng, T. Ding, T. Li, S. Achavananthadith, S. Ahmet, J. S. Ho, G. W. Ho, *Adv. Mater.* **2020**, *32*, 2000351.
[20] M. Sitti, *Nat. Rev. Mater.* **2018**, *3*, 74.
[21] D. Rus, M. T. Tolley, *Nature* **2015**, *521*, 467.
[22] J. del Barrio, C. Sánchez-Somolinos, *Adv. Opt. Mater.* **2019**, *7*, 1900598.
[23] C. A. Spiegel, M. Hippler, A. Münchinger, M. Bastmeyer, C. Barner-Kowollik, M. Wegener, E. Blasco, *Adv. Funct. Mater.* **2020**, *30*, 1907615.
[24] A. Sydney Gladman, E. A. Matsumoto, R. G. Nuzzo, L. Mahadevan, J. A. Lewis, *Nat. Mater.* **2016**, *15*, 413.
[25] F. G. Downs, D. J. Lunn, M. J. Booth, J. B. Sauer, W. J. Ramsay, R. G. Klemperer, C. J. Hawker, H. Bayley, *Nat. Chem.* **2020**, *12*, 363.
[26] T.-Y. Huang, H.-W. Huang, D. D. Jin, Q. Y. Chen, J. Y. Huang, L. Zhang, H. L. Duan, *Sci. Adv.* **2020**, *6*, eaav8219.
[27] H. Jia, E. Mailand, J. Zhou, Z. Huang, G. Dietler, J. M. Kolinski, X. Wang, M. S. Sakar, *Small* **2019**, *15*, 1803870.
[28] M. Lei, W. Hong, Z. Zhao, C. Hamel, M. Chen, H. Lu, H. J. Qi, *ACS Appl. Mater. Interfaces* **2019**, *11*, 22768.
[29] J. W. Boley, W. M. van Rees, C. Lissandrello, M. N. Horenstein, R. L. Truby, A. Kotikian, J. A. Lewis, L. Mahadevan, *Proc. Natl. Acad. Sci. U. S. A.* **2019**, *116*, 20856.
[30] D. Martella, S. Nocentini, D. Nuzhdin, C. Parmeggiani, D. S. Wiersma, *Adv. Mater.* **2017**, *29*, 1704047.
[31] H. Zeng, P. Wasylczyk, C. Parmeggiani, D. Martella, M. Burresi, D. S. Wiersma, *Adv. Mater.* **2015**, *27*, 3883.
[32] C. C. Tartan, J. J. Sandford O'Neill, P. S. Salter, J. Aplinc, M. J. Booth, M. Ravnik, S. M. Morris, S. J. Elston, *Adv. Opt. Mater.* **2018**, *6*, 1800515.
[33] Y. Guo, H. Shahsavan, M. Sitti, *Adv. Mater.* **2020**, *32*, 2002753.
[34] A. Kotikian, R. L. Truby, J. W. Boley, T. J. White, J. A. Lewis, *Adv. Mater.* **2018**, *30*, 1706164.
[35] E. C. Davidson, A. Kotikian, S. Li, J. Aizenberg, J. A. Lewis, *Adv. Mater.* **2020**, *32*, 1905682.
[36] M. López-Valdeolivas, D. Liu, D. J. Broer, C. Sánchez-Somolinos, *Macromol. Rapid Commun.* **2018**, *39*, 1700710.
[37] M. Tabrizi, T. H. Ware, M. R. Shankar, *ACS Appl. Mater. Interfaces* **2019**, *11*, 28236.
[38] Z. Jiang, M. L. Tan, M. Taheri, Q. Yan, T. Tsuzuki, M. G. Gardiner, B. Diggle, L. A. Connal, *Angew. Chem., Int. Ed.* **2020**, *59*, 7049; *Angew. Chem.* **2020**, *132*, 7115.
[39] H. Zeng, H. Zhang, O. Ikkala, A. Priimagi, *Matter* **2020**, *2*, 194.
[40] C. Yang, Z. Suo, *Nat. Rev. Mater.* **2018**, *3*, 125.
[41] F. L. C. Morgan, L. Moroni, M. B. Baker, *Adv. Healthcare Mater.* **2020**, *9*, 1901798.
[42] A. Li, A. Challapalli, G. Li, *Sci. Rep.* **2019**, *9*, 7621.
[43] X. Kuang, K. Chen, C. K. Dunn, J. Wu, V. C. F. Li, H. J. Qi, *ACS Appl. Mater. Interfaces* **2018**, *10*, 7381.
[44] Q. Ge, A. H. Sakhaei, H. Lee, C. K. Dunn, N. X. Fang, M. L. Dunn, *Sci. Rep.* **2016**, *6*, 31110.
[45] S. Tibbits, *Archit. Des.* **2014**, *84*, 116.
[46] Q. Ge, H. J. Qi, M. L. Dunn, *Appl. Phys. Lett.* **2013**, *103*, 131901.
[47] D. Raviv, W. Zhao, C. McKnelly, A. Papadopoulou, A. Kadambi, B. Shi, S. Hirsch, D. Dikovsky, M. Zyracki, C. Olguin, R. Raskar, S. Tibbits, *Sci. Rep.* **2015**, *4*, 7422.
[48] J. M. McCracken, B. R. Donovan, T. J. White, *Adv. Mater.* **2020**, *32*, 1906564.
[49] C. Yan, Q. Yang, G. Li, *Int. J. Mech. Sci.* **2020**, *177*, 105552.
[50] D. J. Broer, C. W. M. Bastiaansen, M. G. Debije, A. P. H. J. Schenning, *Angew. Chem., Int. Ed.* **2012**, *51*, 7102; *Angew. Chem.* **2012**, *124*, 7210.
[51] M. Pilz da Cunha, M. G. Debije, A. P. H. J. Schenning, *Chem. Soc. Rev.* **2020**, *49*, 6568.
[52] T. J. White, M. E. McConney, T. J. Bunning, *J. Mater. Chem.* **2010**, *20*, 9832.
[53] D. J. Mulder, A. P. H. J. Schenning, C. W. M. Bastiaansen, *J. Mater. Chem. C* **2014**, *2*, 6695.
[54] T. J. White, D. J. Broer, *Nat. Mater.* **2015**, *14*, 1087.
[55] J. A. H. P. Sol, G. H. Timmermans, A. J. van Breugel, A. P. H. J. Schenning, M. G. Debije, *Adv. Energy Mater.* **2018**, *8*, 1702922.
[56] F. L. L. Visschers, M. Hendrikx, Y. Zhan, D. Liu, *Soft Matter* **2018**, *14*, 4898.
[57] C. L. Gonzalez, C. W. M. Bastiaansen, J. Lub, J. Loos, K. Lu, H. J. Wondergem, D. J. Broer, *Adv. Mater.* **2008**, *20*, 1246.
[58] A. Kotikian, C. McMahan, E. C. Davidson, J. M. Muhammad, R. D. Weeks, C. Daraio, J. A. Lewis, *Sci. Rob.* **2019**, *4*, eaax7044.
[59] M. del Pozo, C. Delaney, C. W. M. Bastiaansen, D. Diamond, A. P. H. J. Schenning, L. Florea, *ACS Nano* **2020**, *14*, 9832.
[60] L. Ceamanos, Z. Kahveci, M. López-Valdeolivas, D. Liu, D. J. Broer, C. Sánchez-Somolinos, *ACS Appl. Mater. Interfaces* **2020**, *12*, 44195.
[61] M. Javed, S. Tasmim, M. K. Abdelrahman, C. P. Ambulo, T. H. Ware, *Crystals* **2020**, *10*, 420.
[62] R. H. Volpe, D. Mistry, V. V. Patel, R. R. Patel, C. M. Yakacki, *Adv. Healthcare Mater.* **2020**, *9*, 1901136.
[63] H. Yoshida, C. H. Lee, Y. Matsuhisa, A. Fujii, M. Ozaki, *Adv. Mater.* **2007**, *19*, 1187.
[64] J. A. H. P. Sol, H. Sentjens, L. Yang, N. Grossiord, A. P. H. J. Schenning, M. G. Debije, *Adv. Mater.* **2021**, *33*, 2103309.
[65] C. W. Hull, *US4575330A*, **1986**.
[66] S. S. Crump, *US5121329*, **1989**.
[67] C. Zhang, X. Lu, G. Fei, Z. Wang, H. Xia, Y. Zhao, *ACS Appl. Mater. Interfaces* **2019**, *11*, 44774.
[68] L. Chen, Y. Dong, C.-Y. Tang, L. Zhong, W.-C. Law, G. C. P. Tsui, Y. Yang, X. Xie, *ACS Appl. Mater. Interfaces* **2019**, *11*, 19541.
[69] S. Gantenbein, K. Masania, W. Woigk, J. P. W. Sesseg, T. A. Tervoort, A. R. Studart, *Nature* **2018**, *561*, 226.
[70] D. Ahn, L. M. Stevens, K. Zhou, Z. A. Page, *ACS Cent. Sci.* **2020**, *6*, 1555.
[71] M. Rumi, S. Barlow, J. Wang, J. W. Perry, S. R. Marder, *Adv. Polym. Sci.* **2008**, *213*, 1.
[72] X. Zhou, Y. Hou, J. Lin, *AIP Adv.* **2015**, *5*, 030701.

[73] R. J. DeVoe, H. W. Kalweit, C. A. Leatherdale, T. R. Williams, *Proc. SPIE* **2003**, *4797*, 310.
[74] Y. L. Zhang, Q. D. Chen, H. Xia, H. B. Sun, *Nano Today* **2010**, *5*, 435.
[75] A. Selimis, V. Mironov, M. Farsari, *Microelectron. Eng.* **2014**, *132*, 83.
[76] C. P. Ambulo, J. J. Burroughs, J. M. Boothby, H. Kim, M. R. Shankar, T. H. Ware, *ACS Appl. Mater. Interfaces* **2017**, *9*, 37332.
[77] J. Cesarano III, R. Segalman, P. Calvert, *Ceram. Ind.* **1998**, 94.
[78] J. A. Lewis, *Adv. Funct. Mater.* **2006**, *16*, 2193.
[79] J. Planer, *Justus Liebigs Ann. Chem.* **1861**, *118*, 25.
[80] F. Reinitzer, *Monatsh. Chem.* **1888**, *9*, 421.
[81] O. Lehmann, *Z. Phys. Chem.* **1889**, *4*, 462.
[82] G. W. Gray, K. J. Harrison, J. A. Nash, *Electron. Lett.* **1973**, *9*, 130.
[83] G. H. Brown, W. G. Shaw, *Chem. Rev.* **1957**, *57*, 1049.
[84] O. Francescangeli, F. Vita, E. T. Samulski, *Soft Matter* **2014**, *10*, 7685.
[85] D. Liu, D. J. Broer, *Langmuir* **2014**, *30*, 13499.
[86] T. J. White, *J. Polym. Sci., Part B: Polym. Phys.* **2018**, *56*, 695.
[87] A. J. Leadbetter, P. G. Wrighton, *J. Phys., Colloq.* **1979**, *40*, C3.
[88] P. P. C. Verbunt, T. M. de Jong, D. K. G. de Boer, D. J. Broer, M. G. Debije, *Eur. Phys. J.: Appl. Phys.* **2014**, *67*, 10201.
[89] D. M. Agra-Kooijman, M. R. Fisch, S. Kumar, *Liq. Cryst.* **2018**, *45*, 680.
[90] I. Dierking, *Textures of Liquid Crystals*, Wiley-VCH Verlag GmbH & Co. KGaA, Weinheim **2003**.
[91] Y. Zhan, A. P. H. J. Schenning, D. J. Broer, G. Zhou, D. Liu, *Adv. Funct. Mater.* **2018**, *28*, 1707436.
[92] H. Zeng, P. Wasylczyk, G. Cerretti, D. Martella, C. Parmeggiani, D. S. Wiersma, *Appl. Phys. Lett.* **2015**, *106*, 111902.
[93] C. C. Tartan, P. S. Salter, M. J. Booth, S. M. Morris, S. J. Elston, *J. Appl. Phys.* **2016**, *119*, 183106.
[94] C. C. Tartan, P. S. Salter, T. D. Wilkinson, M. J. Booth, S. M. Morris, S. J. Elston, *RSC Adv.* **2017**, *7*, 507.
[95] J. J. Sandford O'Neill, P. S. Salter, M. J. Booth, S. J. Elston, S. M. Morris, *Nat. Commun.* **2020**, *11*, 2203.
[96] W. Feng, D. J. Broer, D. Liu, *Adv. Mater.* **2018**, *30*, 1704970.
[97] D. J. Broer, *Adv. Mater.* **2020**, *32*, 1905144.
[98] D. J. Roach, X. Kuang, C. Yuan, K. Chen, H. J. Qi, *Smart Mater. Struct.* **2018**, *27*, 125011.
[99] P. G. de Gennes, *C. R. Seances Acad. Sci., Ser. B* **1975**, *281*, 101.
[100] D. J. Broer, G. N. Mol, *Polym. Eng. Sci.* **1991**, *31*, 625.
[101] L. T. de Haan, J. M. N. Verjans, D. J. Broer, C. W. M. Bastiaansen, A. P. H. J. Schenning, *J. Am. Chem. Soc.* **2014**, *136*, 10585.
[102] L. T. de Haan, V. Gimenez-Pinto, A. Konya, T.-S. Nguyen, J. M. N. Verjans, C. Sánchez-Somolinos, J. V. Selinger, R. L. B. Selinger, D. J. Broer, A. P. H. J. Schenning, *Adv. Funct. Mater.* **2014**, *24*, 1251.
[103] C. D. Modes, M. Warner, *Phys. Rev. E* **2011**, *84*, 021711.
[104] L. T. de Haan, C. Sánchez-Somolinos, C. W. M. Bastiaansen, A. P. H. J. Schenning, D. J. Broer, *Angew. Chem., Int. Ed.* **2012**, *51*, 12469; *Angew. Chem.* **2012**, *124*, 12637.
[105] T. H. Ware, M. E. McConney, J. J. Wie, V. P. Tondiglia, T. J. White, *Science* **2015**, *347*, 982.
[106] S. Ahn, T. H. Ware, K. M. Lee, V. P. Tondiglia, T. J. White, *Adv. Funct. Mater.* **2016**, *26*, 5819.
[107] S. J. Aßhoff, F. Lancia, S. Iamsaard, B. Matt, T. Kudernac, S. P. Fletcher, N. Katsonis, *Angew. Chem., Int. Ed.* **2017**, *56*, 3261; *Angew. Chem.* **2017**, *129*, 3309.
[108] J. A. H. P. Sol, A. R. Peeketi, N. Vyas, A. P. H. J. Schenning, R. K. Annabattula, M. G. Debije, *Chem. Commun.* **2019**, *55*, 1726.
[109] O. M. Wani, H. Zeng, A. Priimagi, *Nat. Commun.* **2017**, *8*, 15546.
[110] O. M. Wani, R. Verpaalen, H. Zeng, A. Priimagi, A. P. H. J. Schenning, *Adv. Mater.* **2019**, *31*, 1805985.
[111] M. Pilz da Cunha, S. Ambergen, M. G. Debije, E. F. G. A. Homburg, J. M. J. den Toonder, A. P. H. J. Schenning, *Adv. Sci.* **2020**, *7*, 1902842.
[112] M. Pilz da Cunha, H. S. Kandail, J. M. J. den Toonder, A. P. H. J. Schenning, *Proc. Natl. Acad. Sci. U. S. A.* **2020**, *117*, 17571.
[113] C. D. Modes, M. Warner, C. Sánchez-Somolinos, L. T. de Haan, D. Broer, *Proc. R. Soc. A* **2013**, *469*, 20120631.
[114] S. Timoshenko, *J. Opt. Soc. Am.* **1925**, *11*, 233.
[115] J. M. Boothby, T. H. Ware, *Soft Matter* **2017**, *13*, 4349.
[116] K. Kumar, C. Knie, D. Bléger, M. A. Peletier, H. Friedrich, S. Hecht, D. J. Broer, M. G. Debije, A. P. H. J. Schenning, *Nat. Commun.* **2016**, *7*, 11975.
[117] J. E. Stumpel, C. Wouters, N. Herzer, J. Ziegler, D. J. Broer, C. W. M. Bastiaansen, A. P. H. J. Schenning, *Adv. Opt. Mater.* **2014**, *2*, 459.
[118] G. N. Mol, K. D. Harris, C. W. M. Bastiaansen, D. J. Broer, *Adv. Funct. Mater.* **2005**, *15*, 1155.
[119] W. Zhang, A. A. F. Froyen, A. P. H. J. Schenning, G. Zhou, M. G. Debije, L. T. de Haan, *Adv. Photonics Res.* **2021**, *2*, 2100016.
[120] H. K. Bisoyi, Q. Li, *Chem. Rev.* **2016**, *116*, 15089.
[121] M. Pilz da Cunha, E. A. J. van Thoor, M. G. Debije, D. J. Broer, A. P. H. J. Schenning, *J. Mater. Chem. C* **2019**, *7*, 13502.
[122] X. Liu, R. Wei, P. T. Hoang, X. Wang, T. Liu, P. Keller, *Adv. Funct. Mater.* **2015**, *25*, 3022.
[123] N. Torras, K. Zinoviev, C. J. Camargo, H. Campanella, J. Esteve, E. M. Campo, J. E. Marshall, E. M. Terentjev, *Proc. SPIE* **2011**, *8107*, 810704.
[124] Z. Cheng, T. Wang, X. Li, Y. Zhang, H. Yu, *ACS Appl. Mater. Interfaces* **2015**, *7*, 27494.
[125] L. Liu, M. del Pozo, F. Mohseninejad, M. G. Debije, D. J. Broer, A. P. H. J. Schenning, *Adv. Opt. Mater.* **2020**, *8*, 2000732.
[126] M. del Pozo, L. Liu, M. Pilz da Cunha, D. J. Broer, A. P. H. J. Schenning, *Adv. Funct. Mater.* **2020**, *30*, 2005560.
[127] T. S. Hebner, C. N. Bowman, T. J. White, *Polym. Chem.* **2021**, *12*, 1581.
[128] C. Knie, M. Utecht, F. Zhao, H. Kulla, S. Kovalenko, A. M. Brouwer, P. Saalfrank, S. Hecht, D. Bléger, *Chem. Eur. J.* **2014**, *20*, 16492.
[129] A. H. Torbati, P. T. Mather, *J. Polym. Sci., Part B: Polym. Phys.* **2016**, *54*, 38.
[130] K. Kim, Y. Guo, J. Bae, S. Choi, H. Y. Song, S. Park, K. Hyun, S. Ahn, *Small* **2021**, *17*, 2100910.
[131] R. C. P. Verpaalen, M. G. Debije, C. W. M. Bastiaansen, H. Halilović, T. A. P. Engels, A. P. H. J. Schenning, *J. Mater. Chem. A* **2018**, *6*, 17724.
[132] M. J. Ford, C. P. Ambulo, T. A. Kent, E. J. Markvicka, C. Pan, J. Malen, T. H. Ware, C. Majidi, *Proc. Natl. Acad. Sci. U. S. A.* **2019**, *116*, 21438.
[133] M. J. Ford, M. Palaniswamy, C. P. Ambulo, T. H. Ware, C. Majidi, *Soft Matter* **2020**, *16*, 5878.
[134] C. P. Ambulo, M. J. Ford, K. Searles, C. Majidi, T. H. Ware, *ACS Appl. Mater. Interfaces* **2021**, *13*, 12805.
[135] M. Pilz da Cunha, Y. Foelen, T. A. P. Engels, K. Papamichou, M. Hagenbeek, M. G. Debije, A. P. H. J. Schenning, *Adv. Opt. Mater.* **2019**, *7*, 1801604.
[136] M. Pilz da Cunha, Y. Foelen, R. J. H. Raak, J. N. Murphy, T. A. P. Engels, M. G. Debije, A. P. H. J. Schenning, *Adv. Opt. Mater.* **2019**, *7*, 1801643.
[137] H. Ding, Q. Zhang, H. Gu, X. Liu, L. Sun, M. Gu, Z. Gu, *Adv. Funct. Mater.* **2020**, *30*, 1901760.
[138] H. Xia, J. Wang, Y. Tian, Q.-D. Chen, X.-B. Du, Y.-L. Zhang, Y. He, H.-B. Sun, *Adv. Mater.* **2010**, *22*, 3204.
[139] R. K. K. Jayne, T. J. J. Stark, J. B. B. Reeves, D. J. J. Bishop, A. E. E. White, *Adv. Mater. Technol.* **2018**, *3*, 1700293.
[140] J. K. K. Gansel, M. Thiel, M. S. S. Rill, M. Decker, K. Bade, V. Saile, G. Von Freymann, S. Linden, M. Wegener, *Science* **2009**, *325*, 1513.
[141] K. Sugioka, J. Xu, D. Wu, Y. Hanada, Z. Wang, Y. Cheng, K. Midorikawa, *Lab Chip* **2014**, *14*, 3447.
[142] Z. He, Y.-H. Lee, D. Chanda, S.-T. Wu, *Opt. Express* **2018**, *26*, 21184.

[143] K. Tokuoka, H. Yoshida, Y. Miyake, C. H. Lee, Y. Miura, S. Suzuki, A. Fujii, Y. Shimizu, M. Ozaki, *Mol. Cryst. Liq. Cryst.* **2009**, *510*, 126/[1260].
[144] C. H. Lee, H. Yoshida, Y. Miura, A. Fujii, M. Ozaki, *Appl. Phys. Lett.* **2008**, *93*, 173509.
[145] Z. He, G. Tan, D. Chanda, S.-T. Wu, *Opt. Express* **2019**, *27*, 11472.
[146] Z. Ji, X. Zhang, B. Shi, W. Li, W. Luo, I. Drevensek-Olenik, Q. Wu, J. Xu, *Opt. Lett.* **2016**, *41*, 336.
[147] Y. H. Lee, D. Franklin, F. Gou, G. Liu, F. Peng, D. Chanda, S. T. Wu, *Sci. Rep.* **2017**, *7*, 16260.
[148] M. Fleisch, S. Gao, D. Bošnjaković, X. Zhang, R. A. A. Rupp, I. Drevenšek-Olenik, *Liq. Cryst.* **2019**, *46*, 2075.
[149] C. P. Jisha, K.-C. Hsu, Y. Lin, J.-H. Lin, C.-C. Jeng, R.-K. Lee, *Opt. Lett.* **2012**, *37*, 4931.
[150] A. Tudor, C. Delaney, H. Zhang, A. J. Thompson, V. F. Curto, G. Z. Yang, M. J. Higgins, D. Diamond, L. Florea, *Mater. Today* **2018**, *21*, 807.
[151] D. Jin, Q. Chen, T. Y. Huang, J. Huang, L. Zhang, H. Duan, *Mater. Today* **2019**, *32*, 19.
[152] M. Hippler, E. Blasco, J. Qu, M. Tanaka, C. Barner-Kowollik, M. Wegener, M. Bastmeyer, *Nat. Commun.* **2019**, *10*, 232.
[153] A. Nishiguchi, H. Zhang, S. Schweizerhof, M. F. Schulte, A. Mourran, M. Möller, *ACS Appl. Mater. Interfaces* **2020**, *12*, 12176.
[154] A. Nishiguchi, G. Kapiti, J. R. Höhner, S. Singh, M. Moeller, *ACS Appl. Bio Mater.* **2020**, *3*, 2378.
[155] H. Yoshida, C. H. Lee, A. Fujii, M. Ozaki, *Mol. Cryst. Liq. Cryst.* **2007**, *477*, 255.
[156] H. Yoshida, *Liq. Cryst. Today* **2012**, *21*, 3.
[157] I. De Bellis, S. Nocentini, M. G. D. Santi, D. Martella, C. Parmeggiani, S. Zanotto, D. S. Wiersma, *Laser Photonics Rev.* **2021**, 2100090.
[158] J. M. McCracken, V. P. Tondiglia, A. D. Auguste, N. P. Godman, B. R. Donovan, B. N. Bagnall, H. E. Fowler, C. M. Baxter, V. Matavulj, J. D. Berrigan, T. J. White, *Adv. Funct. Mater.* **2019**, *29*, 1903761.
[159] H. Zeng, D. Martella, P. Wasylczyk, G. Cerretti, J.-C. C. G. Lavocat, C.-H. H. Ho, C. Parmeggiani, D. S. Wiersma, *Adv. Mater.* **2014**, *26*, 2319.
[160] S. Nocentini, D. Martella, C. Parmeggiani, D. Wiersma, *Materials* **2016**, *9*, 525.
[161] D. C. Hoekstra, A. P. H. J. Schenning, M. G. Debije, *Soft Matter* **2020**, *16*, 5106.
[162] D. Martella, D. Antonioli, S. Nocentini, D. S. Wiersma, G. Galli, M. Laus, C. Parmeggiani, *RSC Adv.* **2017**, *7*, 19940.
[163] Y. X. Yan, X. T. Tao, Y. H. Sun, C. K. Wang, G. B. Xu, J. X. Yang, Y. Ren, X. Zhao, Y. Z. Wu, X. Q. Yu, M. H. Jiang, *J. Mater. Chem.* **2004**, *14*, 2995.
[164] B. H. Cumpston, S. P. Ananthavel, S. Barlow, D. L. Dyer, J. E. Ehrlich, L. L. Erskine, A. A. Heikal, S. M. Kuebler, I.-Y. S. Y. S. Lee, D. McCord-Maughon, J. Qin, H. Röckel, M. Rumi, X.-L. L. Wu, S. R. Marder, J. W. Perry, *Nature* **1999**, *398*, 51.
[165] K. J. J. Schafer, J. M. M. Hales, M. Balu, K. D. D. Belfield, E. W. W. Van Stryland, D. J. J. Hagan, *J. Photochem. Photobiol., A* **2004**, *162*, 497.
[166] S. Nocentini, D. Martella, C. Parmeggiani, S. Zanotto, D. S. Wiersma, *Adv. Opt. Mater.* **2018**, *6*, 1800167.
[167] S. Nocentini, F. Riboli, M. Burresi, D. Martella, C. Parmeggiani, D. S. Wiersma, *ACS Photonics* **2018**, *5*, 3222.
[168] A. M. Flatae, M. Burresi, H. Zeng, S. Nocentini, S. Wiegele, C. Parmeggiani, H. Kalt, D. Wiersma, *Light: Sci. Appl.* **2015**, *4*, e282.
[169] S. Zanotto, F. Sgrignuoli, S. Nocentini, D. Martella, C. Parmeggiani, D. S. Wiersma, *Appl. Phys. Lett.* **2019**, *114*, 201103.
[170] C. H. Ho, Y. C. Cheng, L. Maigyte, H. Zeng, J. Trull, C. Cojocaru, D. S. Wiersma, K. Staliunas, *Appl. Phys. Lett.* **2015**, *106*, 021113.
[171] Y. Guo, H. Shahsavan, M. Sitti, *Adv. Opt. Mater.* **2020**, *8*, 1902098.
[172] Y. Foelen, D. A. C. van der Heijden, M. del Pozo, J. Lub, C. W. M. Bastiaansen, A. P. H. J. Schenning, *ACS Appl. Mater. Interfaces* **2020**, *12*, 16896.
[173] N. Fomina, C. L. McFearin, M. Sermsakdi, J. M. Morachis, A. Almutairi, *Macromolecules* **2011**, *44*, 8590.
[174] K.-W. Yeung, Y. Dong, L. Chen, C.-Y. Tang, W.-C. Law, G. C.-P. Tsui, D. S. Engstrøm, *Nanotechnol. Rev.* **2020**, *9*, 418.
[175] K. D. Harris, C. W. M. Bastiaansen, D. J. Broer, *J. Microelectromech. Syst.* **2007**, *16*, 480.
[176] H. Khandelwal, G. H. Timmermans, M. G. Debije, A. P. H. J. Schenning, *Chem. Commun.* **2016**, *52*, 10109.
[177] C. A. Smith, *Circuit World* **2008**, *34*, 35.
[178] E. P. Raynes, R. J. A. Tough, K. A. Davies, *Mol. Cryst. Liq. Cryst.* **1979**, *56*, 63.
[179] H. Yoshida, C. H. Lee, A. Fujii, M. Ozaki, *Appl. Phys. Lett.* **2006**, *89*, 231913.
[180] H. Yoshida, Y. Miura, K. Tokuoka, S. Suzuki, A. Fujii, M. Ozaki, *Opt. Express* **2008**, *16*, 19034.
[181] C. A. Koepele, M. Guix, C. Bi, G. Adam, D. J. Cappelleri, *Adv. Intell. Syst.* **2020**, *2*, 1900147.
[182] Z. He, Y.-H. Lee, F. Gou, D. Franklin, D. Chanda, S.-T. Wu, *Opt. Express* **2017**, *25*, 33688.
[183] H. Yoshida, C. H. Lee, Y. Miura, K. Tokuoka, S. Suzuki, A. Fujii, M. Ozaki, *Mol. Cryst. Liq. Cryst.* **2008**, *489*, 73/[399].
[184] Y. Chen, Y. Yin, L. Ma, O. G. Schmidt, *Adv. Opt. Mater.* **2021**, *9*, 2100143.
[185] S. Woska, A. Münchinger, D. Beutel, E. Blasco, J. Hessenauer, O. Karayel, P. Rietz, S. Pfleging, R. Oberle, C. Rockstuhl, M. Wegener, H. Kalt, *Opt. Mater. Express* **2020**, *10*, 2928.
[186] L. Li, Q. Lin, M. Tang, A. J. E. Duncan, C. Ke, *Chem. Eur. J.* **2019**, *25*, 10768.
[187] M. O. Saed, C. P. Ambulo, H. Kim, R. De, V. Raval, K. Searles, D. A. Siddiqui, J. M. O. Cue, M. C. Stefan, M. R. Shankar, T. H. Ware, *Adv. Funct. Mater.* **2019**, *29*, 1806412.
[188] L. L. Ren, B. Li, Y. He, Z. Song, X. Zhou, Q. Liu, L. L. Ren, *ACS Appl. Mater. Interfaces* **2020**, *12*, 15562.
[189] M. Barnes, S. M. Sajadi, S. Parekh, M. M. Rahman, P. M. Ajayan, R. Verduzco, *ACS Appl. Mater. Interfaces* **2020**, *12*, 28692.
[190] Z. Wang, Z. Wang, Y. Zheng, Q. He, Y. Wang, S. Cai, *Sci. Adv.* **2020**, *6*, eabc0034.
[191] T. H. Ware, T. J. White, *Polym. Chem.* **2015**, *6*, 4835.
[192] C. M. Yakacki, M. Saed, D. P. Nair, T. Gong, S. M. Reed, C. N. Bowman, *RSC Adv.* **2015**, *5*, 18997.
[193] H. Wermter, H. Finkelmann, *e-Polymers* **2001**, *1*, 1.
[194] J. W. Chan, C. E. Hoyle, A. B. Lowe, M. Bowman, *Macromolecules* **2010**, *43*, 6381.
[195] A. H. Gelebart, M. K. McBride, A. P. H. J. Schenning, C. N. Bowman, D. J. Broer, *Adv. Funct. Mater.* **2016**, *26*, 5322.
[196] Y. Guo, J. Lee, J. Son, S. Ahn, J.-M. Y. Carrillo, B. G. Sumpter, *Macromolecules* **2019**, *52*, 6878.
[197] J. M. McCracken, B. R. Donovan, K. M. Lynch, T. J. White, *Adv. Funct. Mater.* **2021**, *31*, 2100564.
[198] H.-H. Yoon, D.-Y. Kim, K.-U. Jeong, S. Ahn, *Macromolecules* **2018**, *51*, 1141.
[199] C. P. Ambulo, S. Tasmim, S. Wang, M. K. Abdelrahman, P. E. Zimmern, T. H. Ware, *J. Appl. Phys.* **2020**, *128*, 140901.
[200] R. Rihani, H. Kim, B. Black, R. Atmaramani, M. Saed, J. Pancrazio, T. Ware, *Micromachines* **2018**, *9*, 416.
[201] R. K. Shaha, A. H. Torbati, C. P. Frick, *J. Appl. Polym. Sci.* **2021**, *138*, 50136.
[202] H. Kim, J. M. Boothby, S. Ramachandran, C. D. Lee, T. H. Ware, *Macromolecules* **2017**, *50*, 4267.
[203] M. O. Saed, R. H. Volpe, N. A. Traugutt, R. Visvanathan, N. A. Clark, C. M. Yakacki, *Soft Matter* **2017**, *13*, 7537.

[204] A. O. Konuray, X. Fernández-Francos, À. Serra, X. Ramis, *Eur. Polym. J.* **2016**, *84*, 256.
[205] J. Henricks, C. Ambulo, M. Romero-Ortega, P. Zimmern, T. H. Ware, *J. Urol.* **2019**, *201*, 2019.
[206] S. Tasmim, C. P. Ambulo, M. I. Romero-Ortega, P. E. Zimmern, T. H. Ware, *Neurourol. Urodyn.* **2020**, *39*, S18.
[207] A. S. Kuenstler, Y. Chen, P. Bui, H. Kim, A. DeSimone, L. Jin, R. C. Hayward, *Adv. Mater.* **2020**, *32*, 2000609.
[208] L. Liu, M.-H. Liu, L.-L. Deng, B.-P. Lin, H. Yang, *J. Am. Chem. Soc.* **2017**, *139*, 11333.
[209] B. Zuo, M. Wang, B. Lin, H. Yang, *Nat. Commun.* **2019**, *10*, 4539.
[210] M. Lahikainen, H. Zeng, A. Priimagi, *Nat. Commun.* **2018**, *9*, 4148.
[211] L. Qin, X. Liu, Y. Yu, *Adv. Opt. Mater.* **2021**, *9*, 2001743.
[212] P. Zhang, A. J. J. Kragt, A. P. H. J. Schenning, L. T. de Haan, G. Zhou, *J. Mater. Chem. C* **2018**, *6*, 7184.
[213] P. Zhang, X. Shi, A. P. H. J. Schenning, G. Zhou, L. T. de Haan, *Adv. Mater. Interfaces* **2020**, *7*, 1901878.
[214] P. Zhang, G. Zhou, L. T. de Haan, A. P. H. J. Schenning, *Adv. Funct. Mater.* **2021**, *31*, 2007887.
[215] R. Kizhakidathazhath, Y. Geng, V. S. R. Jampani, C. Charni, A. Sharma, J. P. F. Lagerwall, *Adv. Funct. Mater.* **2020**, *30*, 1909537.
[216] C. Mock-Knoblauch, O. S. Enger, U. D. Schalkowsky, *SID Symp. Dig. Tech. Pap.* **2006**, *37*, 1673.
[217] E. P. A. van Heeswijk, L. Yang, N. Grossiord, A. P. H. J. Schenning, *Adv. Funct. Mater.* **2020**, *30*, 1906833.
[218] Z. Wang, S. Cai, *J. Mater. Chem. B* **2020**, *8*, 6610.
[219] M. O. Saed, A. Gablier, E. M. Terentjev, *Adv. Funct. Mater.* **2020**, *30*, 1906458.
[220] D. W. Hanzon, N. A. Traugutt, M. K. McBride, C. N. Bowman, C. M. Yakacki, K. Yu, *Soft Matter* **2018**, *14*, 951.
[221] Z. Wang, Q. He, Y. Wang, S. Cai, *Soft Matter* **2019**, *15*, 2811.
[222] X. Lu, C. P. Ambulo, S. Wang, L. K. Rivera-Tarazona, H. Kim, K. Searles, T. H. Ware, *Angew. Chem., Int. Ed.* **2021**, *60*, 5536; *Angew. Chem.* **2021**, *133*, 5596.
[223] H. Kwart, I. Burchuk, *J. Am. Chem. Soc.* **1952**, *74*, 3094.
[224] F. H. Beijer, R. P. Sijbesma, H. Kooijman, A. L. Spek, E. W. Meijer, *J. Am. Chem. Soc.* **1998**, *120*, 6761.
[225] M. K. McBride, A. M. Martinez, L. Cox, M. Alim, K. Childress, M. Beiswinger, M. Podgorski, B. T. Worrell, J. Killgore, C. N. Bowman, *Sci. Adv.* **2018**, *4*, eaat4634.
[226] C. Yuan, D. J. Roach, C. K. Dunn, Q. Mu, X. Kuang, C. M. Yakacki, T. J. Wang, K. Yu, H. J. Qi, *Soft Matter* **2017**, *13*, 5558.
[227] D. J. Roach, C. Yuan, X. Kuang, V. C.-F. Li, P. Blake, M. L. Romero, I. Hammel, K. Yu, H. J. Qi, *ACS Appl. Mater. Interfaces* **2019**, *11*, 19514.
[228] M. O. Saed, A. H. Torbati, C. A. Starr, R. Visvanathan, N. A. Clark, C. M. Yakacki, *J. Polym. Sci., Part B: Polym. Phys.* **2017**, *55*, 157.
[229] J. D. W. Madden, N. A. Vandesteeg, P. A. Anquetil, P. G. A. Madden, A. Takshi, R. Z. Pytel, S. R. Lafontaine, P. A. Wieringa, I. W. Hunter, *IEEE J. Oceanic Eng.* **2004**, *29*, 706.
[230] N. A. Traugutt, R. H. Volpe, M. S. Bollinger, M. O. Saed, A. H. Torbati, K. Yu, N. Dadivanyan, C. M. Yakacki, *Soft Matter* **2017**, *13*, 7013.
[231] S. M. Felton, M. T. Tolley, B. Shin, C. D. Onal, E. D. Demaine, D. Rus, R. J. Wood, *Soft Matter* **2013**, *9*, 7688.
[232] R. R. Anderson, J. A. Parrish, *J. Invest. Dermatol.* **1981**, *77*, 13.
[233] J. E. Stumpel, E. R. Gil, A. B. Spoelstra, C. W. M. Bastiaansen, D. J. Broer, A. P. H. J. Schenning, *Adv. Funct. Mater.* **2015**, *25*, 3314.
[234] M. Moirangthem, R. Arts, M. Merkx, A. P. H. J. Schenning, *Adv. Funct. Mater.* **2016**, *26*, 1154.
[235] E. P. A. van Heeswijk, J. J. H. Kloos, N. Grossiord, A. P. H. J. Schenning, *J. Mater. Chem. A* **2019**, *7*, 6113.
[236] A. M. Martinez, M. K. McBride, T. J. White, C. N. Bowman, *Adv. Funct. Mater.* **2020**, *30*, 2003150.
[237] W. Post, A. Susa, R. Blaauw, K. Molenveld, R. J. I. Knoop, *Polym. Rev.* **2020**, *60*, 359.
[238] D. Tanner, J. A. Fitzgerald, B. R. Phillips, *Adv. Mater.* **1989**, *1*, 151.
[239] D. Gräfe, A. Wickberg, M. M. Zieger, M. Wegener, E. Blasco, C. Barner-Kowollik, *Nat. Commun.* **2018**, *9*, 2788.
[240] Y. Liu, P. Wu, *Adv. Funct. Mater.* **2020**, *30*, 2002193.
[241] G. Guidetti, H. Sun, A. Ivanova, B. Marelli, B. Frka-Petesic, *Adv. Sustainable Syst.* **2021**, *5*, 2000272.
[242] L. Yang, A. El-Tamer, U. Hinze, J. Li, Y. Hu, W. Huang, J. Chu, B. N. Chichkov, *Opt. Lasers Eng.* **2015**, *70*, 26.
[243] C. N. LaFratta, L. Li, in *Three-Dimensional Microfabrication Using Two-Photon Polymerization*, Elsevier, Amsterdam **2019**, pp. 385–408.
[244] A. C. Lamont, M. A. Restaino, M. J. Kim, R. D. Sochol, *Lab Chip* **2019**, *19*, 2340.
[245] Y. Yao, J. T. Waters, A. V. Shneidman, J. Cui, X. Wang, N. K. Mandsberg, S. Li, A. C. Balazs, J. Aizenberg, *Proc. Natl. Acad. Sci. U. S. A.* **2018**, *115*, 12950.
[246] J. A. H. P. Sol, L. M. Kessels, M. del Pozo, M. G. Debije, *Adv. Photonics Res.* **2021**, *2*, 2000115.
[247] V. Mazzanti, L. Malagutti, F. Mollica, *Polymers* **2019**, *11*, 1094.
[248] B. Brenken, E. Barocio, A. Favaloro, V. Kunc, R. B. Pipes, *Addit. Manuf.* **2018**, *21*, 1.
[249] P. Calvert, *Chem. Mater.* **2001**, *13*, 3299.
[250] K. Pataky, T. Braschler, A. Negro, P. Renaud, M. P. Lutolf, J. Brugger, *Adv. Mater.* **2012**, *24*, 391.
[251] A. R. Studart, *Chem. Soc. Rev.* **2016**, *45*, 359.
[252] C. L. van Oosten, C. W. M. Bastiaansen, D. J. Broer, *Nat. Mater.* **2009**, *8*, 677.
[253] D. J. Roach, C. M. Hamel, C. K. Dunn, M. V. Johnson, X. Kuang, H. J. Qi, *Addit. Manuf.* **2019**, *29*, 100819.
[254] X. Peng, X. Kuang, D. J. Roach, Y. Wang, C. M. Hamel, C. Lu, H. J. Qi, *Addit. Manuf.* **2021**, *40*, 101911.
[255] A. H. Gelebart, D. J. Mulder, M. Varga, A. Konya, G. Vantomme, E. W. Meijer, R. L. B. Selinger, D. J. Broer, *Nature* **2017**, *546*, 632.
[256] A. R. Peeketi, N. Swaminathan, R. K. Annabattula, *J. Appl. Phys.* **2021**, *129*, 145107.
[257] D. Rus, M. T. Tolley, *Nat. Rev. Mater.* **2018**, *3*, 101.
[258] C. D. Modes, M. Warner, *Europhys. Lett.* **2012**, *97*, 36007.
[259] I. J. Petrick, T. W. Simpson, *Res. Technol. Manag.* **2013**, *56*, 12.

Marc del Pozo obtained his undergraduate degree in Nanotechnology from the Autonomous University of Barcelona in 2015. Later in 2017, he received his Master's degree in Nanomaterials: Chemistry and Physics at Utrecht University. Afterward, he started his Ph.D. studies at the research group of Stimuli-Responsive Functional Materials and Devices under the supervision of Prof. Albert Schenning at the Eindhoven University of Technology (TU/e). He is currently working on the fabrication of 3D printed stimuli-responsive structures based on liquid crystalline polymer networks.

Jeroen A. H. P. Sol received his Bachelor's and Master's degrees in Chemical Engineering and Chemistry from the Eindhoven University of Technology (TU/e), where he graduated *cum laude* on light control in greenhouses using responsive liquid crystalline materials for novel glazing concepts. Subsequently, a doctoral study was started in the same group on the design of stimuli-responsive liquid crystalline inks and exploitation of these for additive manufacturing, guided by Dr. Michael Debije and Prof. Albert Schenning.

Albert P. H. J. Schenning studied chemistry at Radboud University Nijmegen, where he obtained his doctorate in 1996. His Ph.D. thesis was supervised by Dr. Martin Feiters and Prof. Roeland Nolte. In 1996, Schenning was also a postdoctoral fellow in the group of Prof. Bert Meijer at Eindhoven University of Technology (TU/e), working on dendrimers. In 1997, he investigated oligo(triacetylene)s with Prof. François Diederich at ETH Zürich. From 1998 until 2003, Schenning was a fellow of the Royal Netherlands Academy of Arts and Sciences (KNAW). Currently, he is a full professor of stimuli-responsive functional materials and devices at TU/e.

Michael G. Debije received an M.Sc. in High Energy Physics from Iowa State University (U. S. A.) in 1994. He received a Ph.D. in Biophysics from the University of Rochester (U. S. A.) for his study of charge transfer in crystalline DNA oligonucleotides in 2000. In a postdoc position at Delft University of Technology (TUD), he studied charge transport in liquid crystalline discotics and organometallics. In 2003, he joined the Eindhoven University of Technology where he is currently an assistant professor focusing on stimuli-responsive liquid crystalline materials for use in urban architectures, light control, and soft robotics.